JGR Planets

Key Points:

- We performed detailed surface and subsurface mapping of the entire Elysium Planitia region to constrain lava areas, thicknesses, and volumes
- Elysium Planitia is composed of the products of about 40 effusive eruptions including large flood lava flows and lava shields
- Results indicate that there is no singular direction in dike propagation

Supporting Information:

Supporting Information may be found in the online version of this article.

Correspondence to:

J. R. C. Voigt,
voigt@jpl.nasa.gov

Revealing Elysium Planitia's Young Geologic History: Constraints on Lava Emplacement, Areas, and Volumes

J. R. C. Voigt[1,2] , **C. W. Hamilton**[2] , **G. Steinbrügge**[1], **M. S. Christoffersen**[3] , **S. Nerozzi**[2] , **L. Kerber**[1] , **J. W. Holt**[2], and **L. M. Carter**[2]

[1]Jet Propulsion Laboratory, California Institute of Technology, Pasadena, CA, USA, [2]Lunar and Planetary Laboratory, University of Arizona, Tucson, AZ, USA, [3]Geophysical Institute, University of Alaska Fairbanks, Fairbanks, AK, USA

Abstract Elysium Planitia includes several outflow channels that were likely carved by aqueous erosion and subsequently infilled by younger lava flows, making Elysium Planitia the youngest volcanic terrain on Mars. Studying this region is critical for constraining the recent hydrological and thermal evolution of the planet. Here, we investigate the lava flow areas, thicknesses, and volumes in Elysium Planitia using Context (CTX) camera images in combination with SHAllow RADar (SHARAD) sounder data. Compiling 1,777 reflectors over an area of 9,126,790 km^2 allows us to reconstruct the subsurface landscape evolution over time. Our findings show that Elysium Planitia is composed of material from about 40 episodes of effusive volcanic activity. We report volumes for individual eruptions of $4,000 \pm 1,600$ km^3 infilling Athabasca Valles, $12,200 \pm 2,500$ km^3 in Marte Vallis, and $16,000 \pm 4,000$ km^3 in Rahway Valles for the major flow units and volumes as small as 100 ± 50 km^3 in Cerberus Plains. The surface morphologies and inferred dielectric properties of lobe interfaces suggests that the regions consists of basaltic lava. The region also experienced multiple aqueous flooding events. Although, we found evidence of past lava–water interactions, present-day ground-ice (if present) is likely limited to local patches. Further, the pre-eruption landscape reveals that the aqueously carved Marte Vallis is more areal extensive, but shallower than previously suggested, with a likely paleo-flow direction from northwest to southeast. The channel is most likely sourced from a segment in the northwestern portion of Cerberus Fossae, and is now buried by multiple Late Amazonian lavas with the same lava flow direction.

Plain Language Summary Elysium Planitia on Mars has a fascinating history of water and lava flows that shaped its landscape. It is the youngest volcanic terrain on the planet, and studying it helps us to better understand Mars' past as well as recent hydrological and volcanic history. We examined this region by using spacecraft images and radar data to constrain areas, thicknesses, and volumes. An area almost as large as Europe was investigated. The study revealed the products of more than 40 volcanic events, with one of the largest flows infilling Athabasca Valles with a volume of 4,000 km^3. The surface appearance and material properties suggest that Elysium Planitia is composed of basalt, the most common type of lava on Earth. The area also experienced several large floods of water, and there is evidence that lava and water interacted in the past. However, while there could be ice in the ground today, it likely occurs in small patches. The study also provides new insights into the Marte Vallis outflow channel. It seems to be larger, but not as deep as previously thought, with water flowing from northwest to southeast and fed from a fissure in the northwest. Marte Vallis was later covered by several lava layers.

1. Introduction

Elysium Planitia on Mars is a flat-lying plain located south and southeast of the Elysium Rise (e.g., Burr & McEwen, 2000; Burr et al., 2002; Platz & Michael, 2011; Plescia, 2003; Tanaka, 2014; Vaucher, Baratoux, Mangold, et al., 2009). The surface is dominated by Late Amazonian-aged volcanic units that have been modified by aqueous and tectonic activity (Banerdt et al., 2020) as well as aeolian mantling (Ojha et al., 2018). Elysium Planitia is home to several large, partially buried valley systems, including Athabasca Valles, Marte Vallis, Rahway Valles, and Grjótá Valles (e.g., Berman et al., 2001; Jaeger et al., 2007). All valleys are interpreted to be carved by aqueous erosion, subsequently filled with lava flow-fields. Athabasca Valles is interpreted to be filled by lava within the last few million years, making it the most recent volcanically active region on Mars (Jaeger et al., 2010; Vaucher, Baratoux, Mangold, et al., 2009). Marte Vallis, however, is the largest outflow channel to
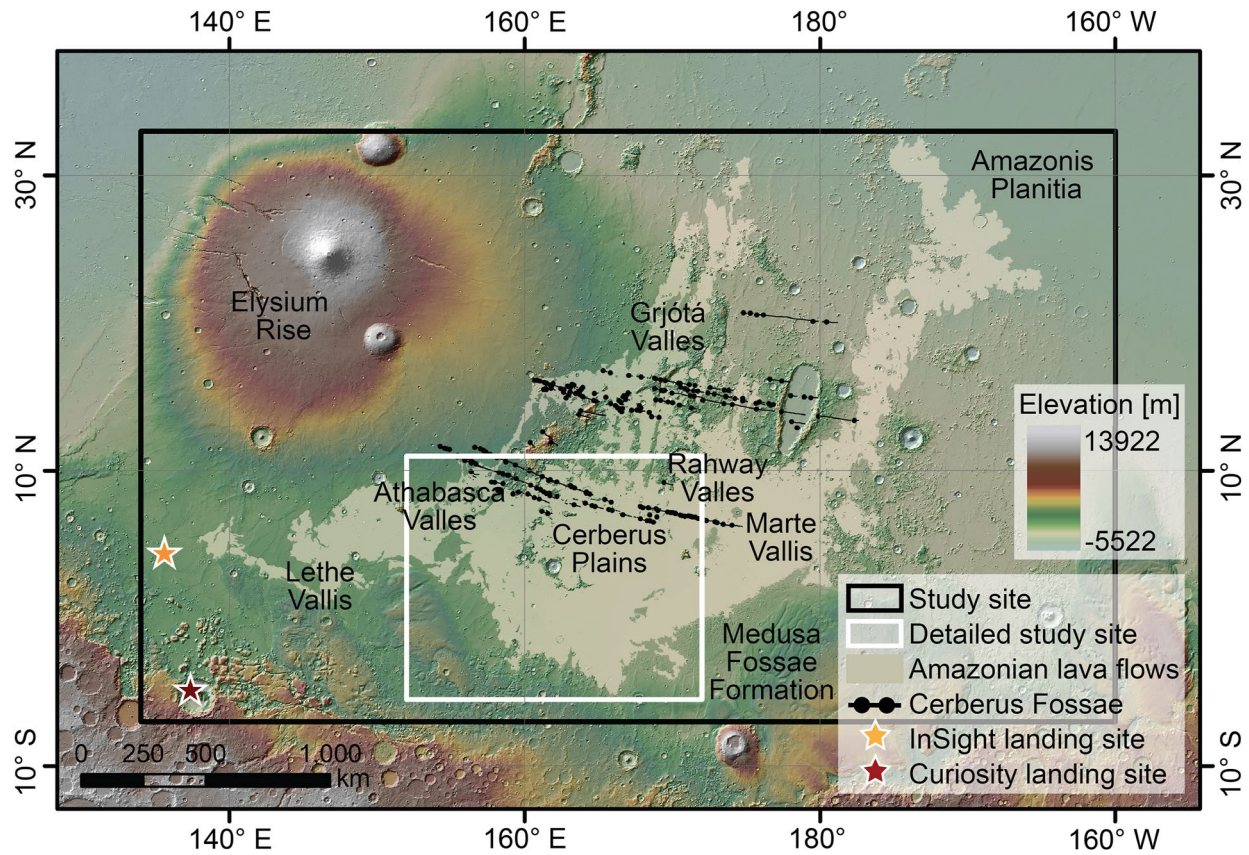
Figure 1. Overview of the study site (black outline) in Elysium Planitia, which is a plains-forming unit in the Elysium and Aeolis quadrangles. Detailed study site (white outline) and major landmarks including the Elysium Rise, Medusae Fossae Formation, Aeolis Planum, Lethe Vallis, Amazonis Planitia, Grjótá Valles, Rahway Valles, Marte Vallis, Cerberus Plains, and Athabasca Valles are shown on a colorized Mars Orbiter Laser Altimeter (MOLA) hillshade. The light-colored beige polygon shows the amazonian-aged lava flows from this study. The *InSight* and *Curiosity* landing sites are marked with an orange and red star, respectively. Different segments of the Cerberus Fossae are marked with black lines with dots.

have been carved within the Late Amazonian epoch on Mars and is now buried by Late Amazonian-aged lavas (Voigt & Hamilton, 2018).

In contrast to the interpretation that Elysium Planitia is mainly composed of volcanic materials (e.g., Hamilton et al., 2010; Jaeger et al., 2007, 2010; Plescia, 2003; Tanaka, 2014; Vaucher, Baratoux, Mangold, et al., 2009; Voigt & Hamilton, 2018), previous studies have also suggested that the platy-structures within Cerberus Plains, initially observed by the High Resolution Stereo Camera (HRSC) onboard *Mars Express* (Jaumann et al., 2007), are related to icy material due to the visual similarity to pack-ice formation on Earth (Murray et al., 2005). More recently, the debate about ice-rich materials infilling the valleys has been resumed based on interpretations of the SHAllow RADar (SHARAD) profiles in terraced craters located within the central part of the Cerberus Plains (Xiong et al., 2021). However, the spectral signature in Elysium Planitia is consistent with volcanic terrains. *Mars Global Surveyor's* Thermal Emission Spectrometer (TES), and *Mars Reconnaissance Orbiter's* (*MRO*) Compact Reconnaissance Imaging Spectrometer for Mars (CRISM) suggest ultramafic to mafic composition (Jaeger et al., 2010; Stockstill-Cahill et al., 2008). The signature from the Neutron Spectrometer component of the Gamma-Ray Spectrometer suite is hydrogen poor (Feldman et al., 2004), and no hydrated minerals have been detected to date by CRISM or Observatoire pour la Minéralogie, l'Eau, les Glaces et l'Activité (OMEGA) in the entire Elysium Planitia region (Mustard et al., 2008; Poulet et al., 2006). Additionally, several in depth characterizations of the surficial materials in different locations in Elysium Planitia argue for an effusive volcanic origin (e.g., Jaeger et al., 2007, 2010; Vaucher, Baratoux, Mangold, et al., 2009; Voigt & Hamilton, 2018).
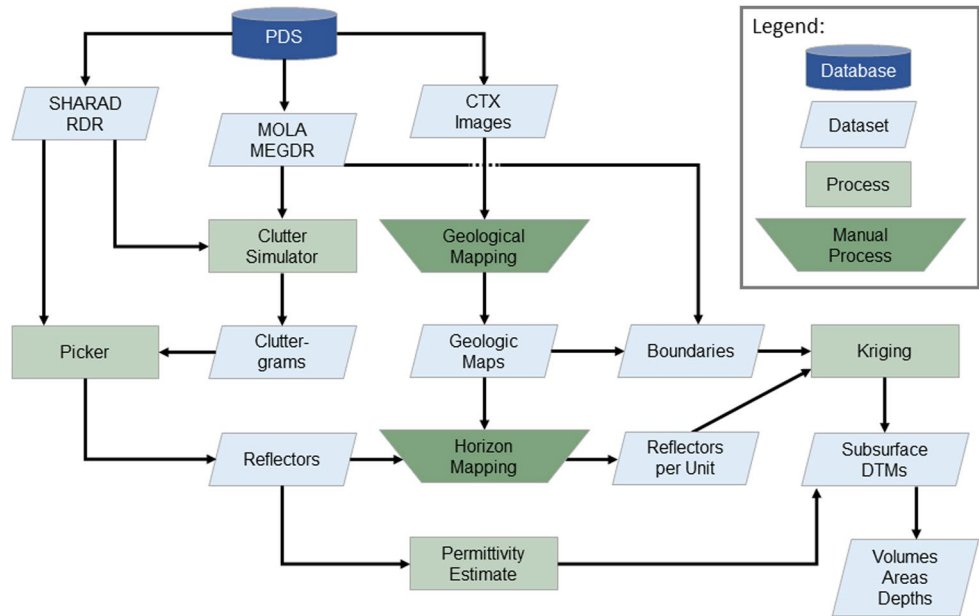
Figure 2. Workflow chart illustrating the used database, data sets, and processes involved in this project.

Elysium Planitia also includes the largest young fissure system on the planet, the Cerberus Fossae. In many cases, the Cerberus Fossae are the source for erupted lava and volatiles. While the origin and concrete process of volcanism on Mars is still debated (Kiefer, 2003; Schumacher & Breuer, 2007), volcanic activity is most commonly explained by longstanding arising mantle-plumes and associated hotspots (Kiefer, 2003) that could still be active today (Broquet & Andrews-Hanna, 2023). An alternative model for the magmatic activity suggests that sufficient heat can be produced by thermal conductivity differences of the crust and mantle resulting in partial melting in the mantle (Schumacher & Breuer, 2007). Additionally, NASA's *Interior Exploration using Seismic Investigations, Geodesy and Heat Transport* (*InSight*) mission detected more than 1,100 seismic events with a majority of events focusing around Cerberus Fossae and the seismicity indicates a warm body of rock beneath Elysium Planitia (Stähler et al., 2022), which is consistent with recent magmatic activity.

Some of the source regions for the release of water and erupting lava are easily traced back to segments of the Cerberus Fossae system, such as for Athabasca Valles where the feeding fissures are located around 10.3°N and 157.0°E. However, for other water releases and lava flow-fields the source regions are less constrained, in particular the location of the fissures that carved and fed Marte Vallis. Currently, there are two contrasting hypotheses: (a) the water was released from a Cerberus Fossae segment in the northwestern part of the Cerberus Plains (e.g., in the surrounding of Athabasca Valles; Berman & Hartmann, 2002; Burr et al., 2002; Fuller & Head, 2002); or (b) the water was sourced by a now buried fissure segment within Marte Vallis. The latter interpretation is supported by Morgan et al. (2013), who investigated parts of Marte Vallis with SHARAD sounding data. The valley system extends over 1,000 km debouching onto Amazonis Planitia in the northeast and with 100 km in diameter, its widest part is located in the Cerberus Plains. However, since Marte Vallis is filled with young lava flows (Voigt & Hamilton, 2018), the main properties of the channel are buried today. The extent, depth, the source, and the lava volume remain poorly constrained (Morgan et al., 2013).

Here, we map the individual lava flows throughout entire Elysium Planitia (Figure 1) to reconstruct the volcanic evolution of the region and the emplacement dynamics of the flows. In Section 2, we provide detailed information about our methodology. In Section 3, we present the results of the surface mapping. Section 4 presents the results of the subsurface investigation in which we mapped all reflectors within Elysium Planitia using SHARAD sounding data. In turn, this information allows us to constrain the dielectric properties of the lava to generate thickness estimates for individual flow units. Combining surface and subsurface topography, we then derive erupted lava volumes in Section 5. The relative emplacement of the individual flows and surface characteristics provide further inside into the young geologic history of the region, which is discussed in Section 6.

2. Data and Methods

2.1. Surface Analysis

The primary objectives of the surface analysis are to constrain the areas of the individual volcanic eruptions, identify lava flow directions, and source regions. The surface characteristics were mainly determined based on images obtained from the Context (CTX) camera (Malin et al., 2007) onboard the *Mars Reconnaissance Orbiter* (*MRO*) (Figure 2). Two different CTX data products are used, including single CTX images and the new global CTX basemap generated by Dickson et al. (2018, 2023). Both CTX products have a resolution of 6 m/pixel. In selected areas, we combine our observations with *MRO* High Resolution Imaging Science Experiment (HiRISE) images, with a resolution of 0.3 m/pixel (McEwen et al., 2007). To obtain topographic information, we use the Mission Experiment Gridded Data Records (MEGDRs) with a horizontal resolution at the equator of 463 m/pixel from the Mars Orbiter Laser Altimeter (MOLA) onboard the *Mars Global Surveyor* (*MGS*) (Smith et al., 2001). The remote sensing data were imported into the geographic information system (GIS), Environmental Systems Research Institute (ESRI) ArcGIS version 10.7.1, to create geomorphological maps.

Two different maps were generated: (a) a map that illustrates the spatial distribution of the Late Amazonian volcanic terrains with its major flow units (Figure 3) and (b) a lava flow map that focuses on lava flow margins within the Late Amazonian volcanic terrain in the Cerberus Plains (Figure 6). The former map illustrates the geologic contact of the lava flow-fields with other geologic units including Amazonian, Hesperian, and Noachian-aged terrains. For simplification, we will refer to this map as "the geologic contact map" from here on. Please note that this map is not a complete geologic map and rather illustrates the geologic contacts between the relevant lava flow-fields and older terrains. The digitizing scale of the geologic contact map is 1:100,000. The second map contains lava flow margins that we interpret to represent different volcanic eruptions within the Middle and Late Amazonian epochs. The map focuses on the central part of Elysium Planitia, Cerberus Plains, where multiple lava flow-fields with distinct characteristics occur, including multiple smaller lava shields, lava flow-fields, and flood basalts. This second map is referred to as the "flow unit map." Since this region requires a
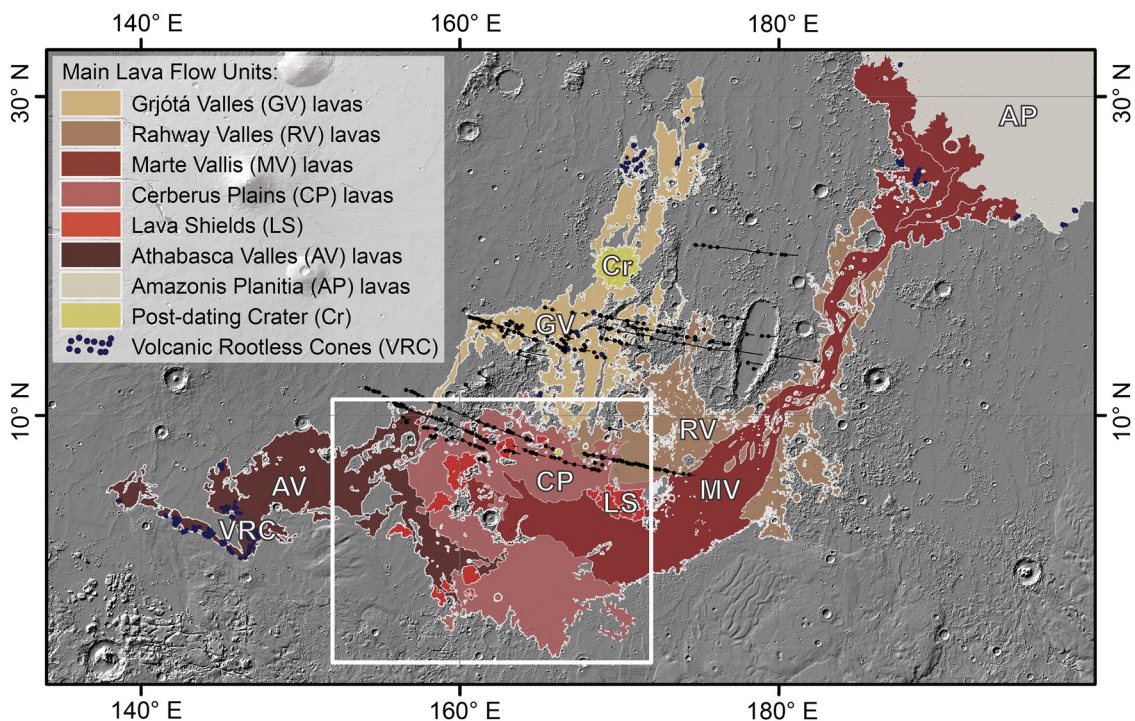
Figure 3. Map showing the major lava flow units in Elysium Planitia namely: Grjótá Valles (GV) lavas, Rahway Valles (RV) lavas, Marte Vallis (MV) lavas, Cerberus Plains (CP) lavas, and Athabasca Valles (AV) lavas. The map also shows the location of the Lava Shields (LS) within the Cerberus Plains, Amazonis Planitia (AV) lavas in the northeast, Volcanic rootless cones (VRC), and post-dating impact Craters (Cr) including Kota and Zunil. The detailed study site focusing on the central part of Cerberus Plains showing in Figure 6 is contoured by a white outline. Color-coded lava flow units are overlain on a MOLA hillshade and were digitized on a 1:100,000 scale based on CTX images.
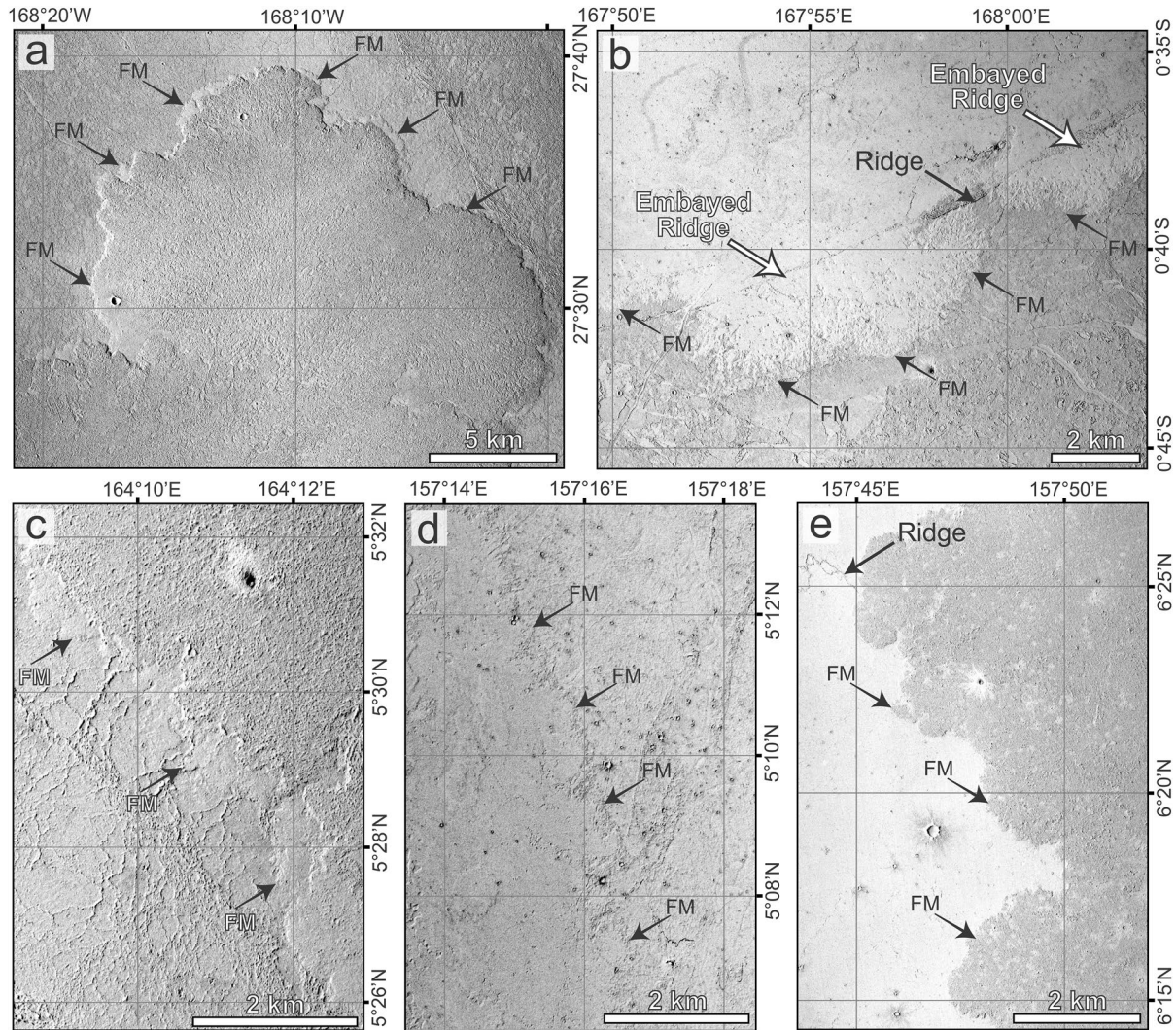
Figure 4. Examples of typical flow margins in Elysium Planitia as seen by CTX. Black arrows point toward the flow margin (FM) of the younger flow. White arrow indicate features that formed by the older flow and were partially (panel b) or completely (panel e) overprinted by the younger flow. (a) Flow margins at the distal end of the Marte Vallis lava with disrupted crust lies on Amazonis Planitia lavas with disrupted crust. Often Marte Vallis lavas formed small peripheral breakouts with smooth and continuous crust. (b) Smooth and continuous lava crust of the CP_{19} lava unit lies on disrupted CP_{18} lava crust. Note how the smooth lava unit partially embays the ridge of the underlying lava surface (marked by white arrows). (c) Contact of $CP_9$ and Marte Vallis lavas in Cerberus Plains. CP_9 lava unit exhibits dominantly highly disrupted surfaces surrounded by breakouts with smooth and continuous crust emplaced on to Marte Vallis lavas with disrupted surfaces. (d) Smooth and continuous crust of Athabasca Valles lavas overlies smooth and continuous crust of CP_{11} lava. (e) Disrupted crust of the CP_{13} lava unit lies on smooth and continuous CP_{12} lava crust.

more intense mapping approach the digitizing scale was set to 1:80,000 to capture slight changes in surface characteristics, such as facies changes including surface roughness (Voigt, Hamilton, Steinbrügge, & Scheidt, 2021), lobe scale changes, cross-cutting relationships, and relative crater population. Our mapping approach is a factor of 80 times higher than previous maps (map scale of 1:1,770,000; Vaucher, Baratoux, Mangold, et al., 2009) and covers the entire Elysium Planitia region. Both maps show three different contact types using polylines that indicate certain, approximate, and uncertain boundaries, which are marked with solid, dashed, and dotted lines, respectively. The two maps were created based on variations in albedo, texture, and shape (i.e., geomorphology). Very specific facies were used to help defining flow units. A major indicator to distinguish two flow units was when smooth facies was surrounding a rough facies, indicative of late stage breakouts (Figures 4a and 4c). Another example is the positive relief features, curvilinear ridges, in Rahway Valles. This facies helped to identify that Rahway Valles lava are exposed in the south of Marte Vallis lavas, as well as have surface exposures

within Marte Vallis ("streamlined islands"). Additionally, we used kinematic indicators showing flow directions to define flow units as well as overlapping relationships. However, in some cases it is complicated to distinguish between different branches produced by one eruption versus two separate eruptions, as overprinting of earlier lobes, still shows a stratigraphic difference. Often bigger obstacles divide the lava flow-field or the pre-eruption topography affects the lava pathways which resulted in distinct surface characteristics despite being the same flow. In some locations, the subsurface reflectors help identifying the real stratigraphy. In selected areas, we used crater size–frequency distributions (CSFDs) to determine the crater retention ages of the surface to help to identify the units identity. However, since the study site is very large (1,623,518 km²) it was not feasible to create a chronological sequence of geological events based on CSFDs within this study. Instead, the CSFDs were used as an additional tool to define very specific units (e.g., the surface exposures in shape of islands within Marte Vallis). For this purpose, we digitized craters with a diameter larger than 50 m and used the CraterTools software in ArcGIS from the Freie Universität Berlin (Kneissl et al., 2011) as well as Craterstats 2.0 (Michael, 2013; Michael & Neukum, 2010) to manage the data.

2.2. Subsurface Analysis

To determine the lava flow thicknesses within Elysium Planitia, we analyzed reflectors obtained from the SHAllow RADar (SHARAD) sounder (Seu et al., 2007) onboard *MRO*. This study uses the US Radar Data Record (USRDR), which is publicly available on the NASA Planetary Data System (PDS). The investigation area has been limited in latitude from 33°N to 7°S and from 134° to 200°E in longitude. As of the time we conducted the study, 2,106 tracks pass through this selected area and all radargrams have been cut to the study area using the geometry files associated with the data product (USGEOM). The trimmed radargrams have been loaded into a picker software where they can be visually compared to incoherent cluttergrams derived from the MOLA gridded data product (Choudhary et al., 2016; Holt et al., 2008). Picks have been chosen manually using direct comparison to surface clutter simulations to avoid false picks and special attention has been paid to avoiding side lobes due to the shallow nature of many reflectors. The input to the picker is an upper and lower boundary for each layer from where it picks the brightest pixel within the selected zone of each range line. If a reflector was present, the surface had to be picked as well, to calculate the reflector depth.

The set of chosen reflectors was post-processed by retrieving the difference in samples between each reflector pixel and the overlaying surface, leading to a depth profile along-track. The depth in samples can be converted into physical units for using the real part of the relative dielectric permittivity ε' (in the following referred to as permittivity), by using the speed of light in a medium

$$v = c/\sqrt{\varepsilon'}, \tag{1}$$

where c is the speed of light in vacuum. The depth of the reflector can then be computed from the two-way time of flight

$$d = vt\Delta s/2, \tag{2}$$

where Δs is the depth in samples and t is the SHARAD sampling interval of 0.0375 μs.

To assign and connect the reflectors to their flow unit seen on the surface, we labeled each reflector associated to the flow unit above. For this approach, we used the flow units resulting from the surface mapping (e.g., Figures 3 and 6) in combination with the sample number (depth) and shape of the reflector. In cases with stacked reflectors and reflectors where the flow unit is not exposed at the surface, we started with regions where the surface of the flow unit was exposed and easy to assign in the radargram (where possible) and then followed the horizon of the reflector along the subsurface. With this approach the large majority of reflectors could be assigned. Problematic to label and define are deep short reflectors that seem to be segmented and where we do not see an obvious surface exposure. These reflectors correspond to deeper and presumably older interfaces and are less important to constrain within this study.

To assess the permittivity, we studied locations where a lava lobe flowed onto, but did not completely cover, a flat surface. In this configuration the reflector underneath the flow tends to bend downwards due to the reduced speed of light in the medium (see Figure 7 for an example). We then assumed that the dipping-reflector is at the same elevation than the uncovered portion of the flat surface. Under this specific geometric assumption, the radar wave speed, and therefore also the real part of the permittivity, can be estimated.

We used Bayesian inference (Sivia & Skilling, 2006) to estimate the permittivity of three different units within the study area. We began each inversion with a uniform prior probability density function (PDF) over permittivity between 1 and 20. We then calculated a Gaussian likelihood over permittivity for each reflector in a unit using the difference between the assumed elevation and the calculated reflector elevation at a given permittivity. With each likelihood we apply Bayes' theorem to iteratively update a posterior PDF over permittivity. We report summary measures from the final posterior PDF for each unit.

At flow boundaries where the reflectors were too shallow to be identified we complemented the data set by using MOLA to constrain the thickness of the flows at the distal extent, where the lava flow was stratigraphically and topographically higher than the surroundings. This method works well, when lava lobes are emplaced onto flat plains, however, it does not allow us to place additional constraints in geologic settings where the lava was emplaced in a topographically confined location, such as in the previously carved valleys in the proximal part of Athabasaca Valles.

The depth profiles from the SHARAD data set were then interpolated to create digital terrain models (DTMs) for each flow unit using Ordinary Kriging (Wackernagel, 1995). Kriging is generally considered to be the most accurate method for spatial topography interpolation (Arun, 2013); however, results still vary as a function of data density, data quality, and the nature of the subsurface topography. Together with the interpolated depth values, the method returns the variance at the specified grid points which is used for the error propagation. The interpolation has been limited to the projected extent of the subsurface flows. Areas past the flow fronts identified in the surface mapping have been masked using the shapefiles for the respective units. Further, we have not extrapolated any flows, so in some regions the extent of the DTM is limited by data availability. Subsurface maps indicating the relative depth of the subsurface with respect to the surface topography for the respective flow units are provided in the supplementary material with pixel scales of either 500, 1,000, or 5,000 m/px, dependent on the size of the flow, in an equidistant projection.

To compute the volumes of lava flows, overlaying units, if present, have been subtracted from the subsurface DTM to convert reflector depths to thicknesses. To perform this operation it was required to have all units at the same pixel scale. Therefore, all lava volumes have been computed on a 5,000 m/px resolution. The volume errors have been assessed from the uncertainty in the permittivity and the per pixel variance of the measured depth as given by the Kriging algorithm. We propagated these into a volume and average depth error by performing a Monte Carlo simulation using 5,000 realizations for each unit. For each realization the depth of each pixel in the subsurface DTM was randomized according to its respective error and the permittivity was randomized per unit. An example for Marte Vallis is shown in the supplementary material with the depth errors shown in Figure S1 and the resulting volume distributions in Figure S2 of the Supporting Information S1.

3. Surface Mapping

The major geologic units forming Elysium Planitia can be divided into five broad groups: Grjótá Valles lavas, Rahway Valles lavas, Marte Vallis lavas, Cerberus Plains lavas, and Athabasca Valles lavas (Figure 3). All five groups belong to geologic units previously described by Tanaka et al. (2005), namely the Cerberus Fossae 2 and 3 units (AEc_2 and AEc_3). However, these units have also been described as the Amazonian Cerberus old and young units (ACo and ACy) by Vaucher, Baratoux, Mangold, et al. (2009) and were grouped together into a single late Amazonian volcanic (lAv) unit by Tanaka (2014). In this study, unit boundaries are informed by previous studies, but all of our contacts were digitized as original work using higher resolution basemaps (6 m/px) and at finer mapping scales (1:80,000–1:100,000).

Our mapping results show that the lava flow-fields cover a total spatial area of 1,623,518 km^2, corresponding to 1.12% of Mars' surface area. Note, we use the term "Cerberus Plains lava" to refer to the lava flows in the central part of Elysium Planitia which are not belonging to the large flood basalts infilling Athabasca Valles and Marte Vallis. While from a geographical point of view the proximal part and southeastern branch of Athabasca Valles lavas as well as the proximal part of Marte Vallis lava lie within Cerberus Plains, Athabasca Valles, and Marte Vallis lava are separate flood units. Only the smaller lava flow-fields are grouped together into Cerberus Plains lava unit.

3.1. Grjótá Valles Lavas

Grjótá Valles lavas are located in the northern part of Elysium Planitia. The unit has an exposed area of 234,260 km^2, but is likely buried in the south. It has surficial exposed contacts to Athabasca Valles lavas, lavas

forming the Cerberus Plains, and the northern part of Rahway Valles lavas. The morphological characteristics highly vary throughout the area. Most flow indicators imply that the majority of this unit was fed from fissure segments associated with Grjótá Valles forming lava flows emplaced toward the south and north. Close to the vent area, the lava is only decimeters up to a few meters thick, appearing to coat the terrain. These flows, hereafter referred to as lava veneers, may be associated with low viscosities during the emplacement and are too thin to be resolved by SHARAD data. Lava in the vent-proximal part is mainly embaying older and larger craters and shows a high distribution of secondary craters associated with the Kota impact crater. Kota crater divides Grjótá Valles lavas into a northern and southern part. Close to Kota crater, the lava contact is covered by the ejecta material and thus a continuous connection to the north is not exposed. In contrast to the lava surfaces in the proximal part, the most northern flow margins show a very different morphological character. The flow margins are comparably thick and show evidence of inflation, including tumuli, inflation plateaus and prominent clefts, as well as inflation pits. The northern parts of the flow-field also show evidence of different lava levels that most likely suggest lava ponding, subsequently followed by a drainage event. In the north, the Grjótá Valles lava was also emplaced onto older lavas, showing characteristics associated with higher flow viscosities with a northwest to southeast flow direction, likely Elysium Mons lava flows. This complex lava relationship between older Elysium Rise flows and younger Grjótá Valles lava sometimes leads to challenges identifying flow contacts and morphological characteristics. Underlying flow units are covered with thin lava veneers while the older units are still visible and not completely modified by the younger Grjótá Valles lavas. The northern part of Grjótá Valles lava exhibits a large population of volcanic rootless cones (Hamilton et al., 2010, 2011, 2013) indicating lava–water or lava–ground-ice interaction during the time of emplacement. In general, volcanic rootless cones (constructs formed by phreatovolcanic activity) are found throughout the unit with the exception of the western extent (e.g., in the central part close to Grjótá Valles segments, eastern extent, and southern part). Major rootless cone populations are indicated by blue dots in Figure 3. Generally, the Grjótá Valles lava seemed to be the oldest exposure within Elysium Planitia lavas belonging to the AEc_2 unit with surface ages of ~125 Ma (Hamilton et al., 2010).

Recently, Brown and Roberts (2023) investigated the morphological character of Grjótá Valles and concluded that five channels were carved by catastrophic aqueous flow processes (or maybe turbulent lava emplacement) sourced from the faults system with a propagation eastwards. The conclusion that the last geologic event was an aqueous carving event producing the channels was based on the lack of features suggesting that the channel might have been filled by lava afterward. However, the lack of prominent lava features such as inflation pits and plateaus or "platy ridged" terrain (Keszthelyi et al., 2004) can be due to the proximity to the source region. Close to the vent there is often a thin veneer of lava present and thus the surface often mimics previously formed morphologies, such as eroded channels. In Athabasca Valles for example, we see dominant volcanic features with distance from the vent, whereas in proximal regions no prominent volcanic features are present such as lobate margins, platy ridged, volcanic rootless cones, or inflation features. Similarly, in the proximity of the fossae segments that were feeding the Grjótá Valles region we identified thin veneers of lava. We agree with previous interpretations by Burr et al. (2002) and Brown and Roberts (2023) that the channels were initially carved by water (or perhaps turbulent lava), but the surface material and latest geological event is likely not fluvial. Instead, we argue that close to the vent a thin veneer of lava is present which could have been due to a drainage event leaving behind "bathtub rings," previously identified by Brown and Roberts (2023). However, they interpreted the "bathtub rings" and entire unit to be aqueous in origin, whereas we interpret that the morphologies, such as the "bathtub rings" in the proximal part and prominent lobes with inflation features in the distal part are consistent with lava features and thus favor a volcanic origin.

3.2. Rahway Valles Lavas

Rahway Valles lavas are located north and south of the central Marte Vallis and have a total exposed surface area of 272,252 km^2. This unit has direct contacts with Grjótá Valles lavas, Marte Vallis lavas, and Cerberus Plains lavas. The morphological character is described in detail by Voigt and Hamilton (2018) and, based on CSFDs, the surface is estimated to have an age of 20 Ma, which implies that it is an older part of the AEc_3 unit, but not a part of the AEc_2 unit (Voigt & Hamilton, 2018). Most of the lava seems to have been fed by the eastern part of the Cerberus Fossae (around 7°N and 171°E), forming lava fields flowing toward the northeast and infilling the southern portion of Rahway Valles. Since there are exposures of the unit south of Marte Vallis and localized "islands" (i.e., kīpuka) within Marte Vallis, we interpret that the initial flow direction was also toward the southeast creating Rahway Valles lavas that are now partially covered by younger Marte Vallis lavas. In addition to the
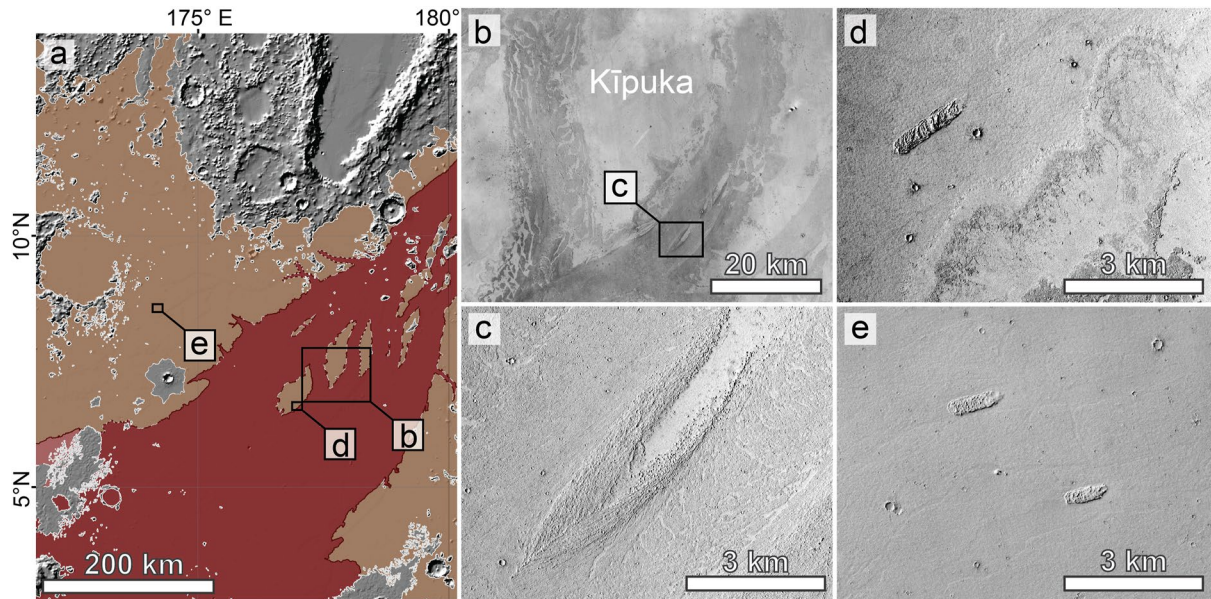
Figure 5. Examples of flow morphologies of Rahway Valles and Marte Vallis lavas. (a) Overview of Rahway Valles lavas and Marte Vallis lavas color-coded as Figures 3 and 6 overlain on MOLA hillshade. (b) CTX mosaic from Dickson et al. (2018) of kīpuka belonging to the Rahway Valles lavas and are embayed by the younger Marte Vallis flow. (c) Facies called "furrowed arcuate ridges with tail" (Voigt & Hamilton, 2018) presents a good indicator of the lava flow direction, from southwest toward northeast. (d) and (e) Facies called "furrowed arcuate ridges without tail (F.1.2)" described in Voigt and Hamilton (2018) as seen by CTX. (d) The F.1.2 facies is located on kīpuka, which are embayed by the younger Marte Vallis lavas in the southeastern part of this panel. (e) "Furrowed arcuate ridges without tail (F.1.2)" in the northern part of Rahway Valles.

main feeder vent(s) associated with the Cerberus Fossae segments, there are at least two other smaller vents that are currently exposed at the surface in the northern part of Rahway Valles around 13°N and 173°E. These vents appear to have fed lava that flowed southwest and southeast. Even though Rahway Valles may have been modified by fluvial and/or periglacial processes (Ramsdale et al., 2015), the Rahway Valles lavas do not show any evidence of lava–water/ice interaction during the lava emplacement to form volcanic rootless cones. The central part of Marte Vallis (around 7°N and 177°E) exhibits "streamlined islands" (hereafter referred to as "kīpuka," Figures 5a and 5b). These surface expressions could represent a different lava facies, or a different geologic unit compared to the surrounding lavas infilling Marte Vallis. Detailed morphological investigation revealed that the surface exhibits features often seen in the northern part of Rahway Valles, namely "furrowed arcuate ridges without tail (F.1.2)" described in Voigt and Hamilton (2018) and Figure 9 therein. These "furrowed arcuate ridges without tail (F.1.2)" are mostly surrounded by a very smooth surface exhibiting lightly defined polygons (Figures 5d and 5e). Additionally, the kīpuka are bounded by lobate margins, indicating a younger flow (i.e., Marte Vallis lavas) embaying the slightly higher-standing kīpuka (Figure 5d). These flow margins could represent a late stage of the flow emplacement, where the initial lava covered the kīpuka and left behind a thin veneer. However, our CSFDs reveal a surface age of the kīpuka of about 20 Ma years, which is consistent with the surface age of the northern exposure of Rahway Valles, which is estimated to be 20 Ma (Voigt & Hamilton, 2018). Thus, we conclude that the surface of the kīpuka represent the older Rahway Valles lavas that are partially embayed (but not completely covered) by the younger Marte Vallis lavas.

3.3. Marte Vallis Lavas

Marte Vallis lavas are located in the central eastern and most eastern part of Elysium Planitia and have an exposed surface area of 491,767 km^2. Lavas infilling Marte Vallis show surficial contacts with Rahway Valles and Cerberus Plains lavas. Marte Vallis lavas represent the most eastern extent of Elysium Planitia, where lavas debouch onto Amazonis Planitia to form flows with mostly well-defined margins. Well-defined flow margins can also be found in contact with Rahway Valles lavas in the north and south of Marte Vallis. The central part of Marte Vallis lavas is described in detail by Voigt and Hamilton (2018), and lava morphologies exhibit a high variety of lava textures including but not limited to: highly disrupted lava crust exhibiting wakes and forming
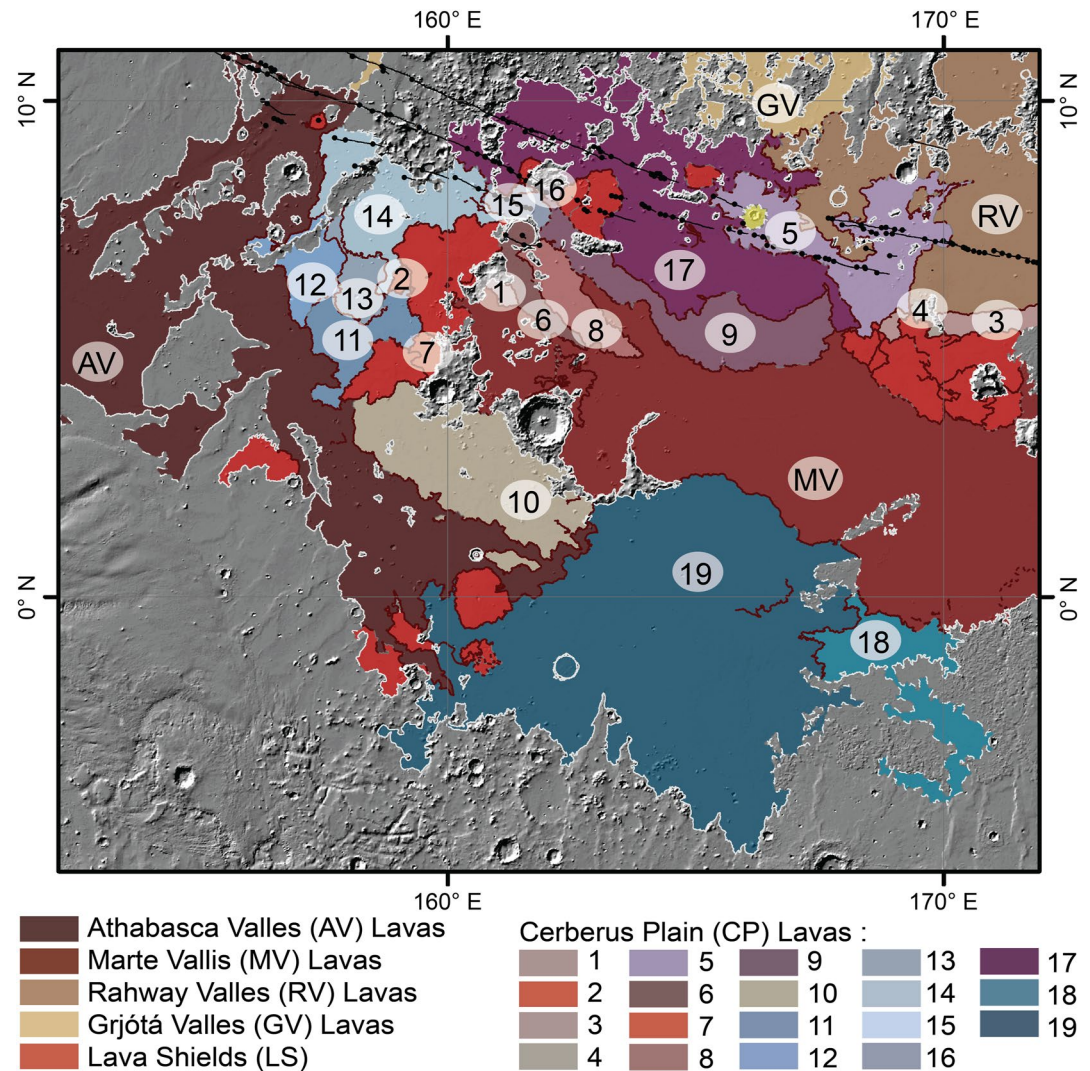
Figure 6. Overview of lava flow-fields, in different shades of red, pink, purple, and blue labeled by number, and lava shields marked in bright red composing the Cerberus Plains. Note, that CP_2 and CP_7 might represent an earlier stage of lava shield activities and thus are shown in bright red. The adjacent major lava flows GV, RV, MV, and AV are shown in the same color as in Figure 3. The flow margins were digitized on CTX images at a 1:80,000 scale and are shown here on a MOLA hillshade.

islands; smooth and continuous lava crust with evidence of inflation showing inflation plateaus and pits as well as polygonal patterned terrains; and platy-ridged terrains. Most of these lava facies can be used to infer flow directions, such as "lava islands" that are described as "furrowed arcuate ridges with tail" (Voigt & Hamilton, 2018), where the tail is formed in the down flow direction (Figure 5c). Please note that teardrop-shaped "lava islands" differ from kīpuka in that the surface is mantled by lava. Lava "plates" commonly form at the side of the underlying valley (Voigt & Hamilton, 2018). These lava facies can be continuously traced throughout the proximal and central part of Marte Vallis, indicating that the lava surface was formed during one eruption. Based on multiple flow indicators seen on the lava surface in combination with our SHARAD investigation, we interpret that the lava infilling Marte Vallis was fed by a segment of Cerberus Fossae that is now buried by younger flow-fields in the Cerberus Plains (around 8°N and 161°E). With a surface age of 9 Ma (Voigt & Hamilton, 2018), lavas infilling Marte Vallis are younger than in Rahway Valles and Grjótá Valles and are defined to be part of the AEc_3 geologic unit in Tanaka et al. (2005). This is also reflected in the stratigraphic relationship to Rahway Valles lavas, where Marte Vallis lavas are overlapping the Rahway Valles lavas. Good examples are located along the northern contact. The distal end is divided into two main lava branches that exhibit the same morphological
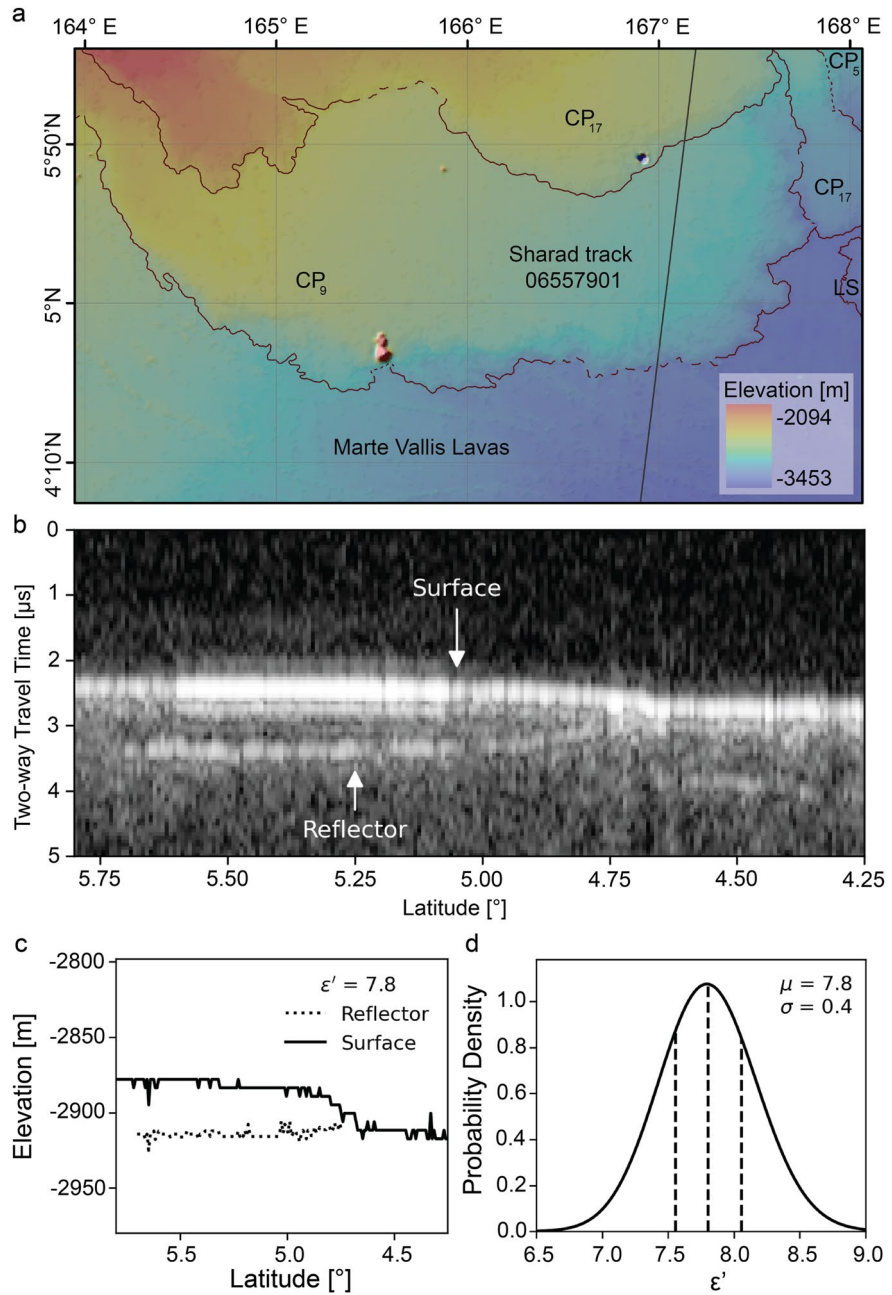
Figure 7. Dipping Reflector Example. (a) Location of CP_9 unit used to calculate permittivity by dipping reflectors overlain by color-coded MOLA DTM. Note that CP_9 overlaps Marte Vallis lavas (MV). Black line represents the ground track from the radargram in (b) Sharad ID 06557901. (c) Shows the base (after depth calculation) and surface of the CP_9 flow unit as well as the surface of the flow (MV). (d) Probability distribution over permittivity after analyzing near-margin reflectors in CP_9 unit, showing a mean, μ, of 7.8 and its uncertainty, σ, of 0.4.

characteristics, being highly disrupted with smooth surfaced breakouts around the flow margin. At least three possible scenarios can create the observed morphologies: (a) The most distal end was overridden by a newer lava flow that stalled a few tens to hundreds of kilometers before reaching its most eastern extent. In that case, the most distal branch would be stratigraphically older. (b) The most distal flow front was overriding an initially emplaced lava flow that stalled earlier (most distal end is younger). (c) The most distal part belongs to the much older Rahway Valles lavas. Based on our observations, the third scenario is less likely because the morphology is more similar to the Marte Vallis lavas and the crater density appears similar for the two branches. However,

additional investigations would be necessary to conclude which of the three scenarios is most likely. Within the proximal and central part of Marte Vallis, no rootless cones are exposed and thus there is no direct evidence of lava–water/ice interactions during the time of emplacement in the valley itself. However, explosive interactions do not always result from interactions between lava and volatiles, and rootless cone populations are found in the distal end close to 25°N and 171°W (Figure 3).

3.4. Cerberus Plains Lavas

Cerberus Plains lavas are located in the central part of Elysium Planitia and cover an exposed area of 271,131 km^2 with 48,656 km^2 of it forming Lava Shields (marked in bright red in Figures 3 and 6). The Cerberus Plains lavas are in contact with Grjótá Valles lavas, Rahway Valles lavas, Marte Vallis lavas, and Athabasca Valles lavas and thus Cerberus Plain lavas represent the only unit sharing contacts with all other lava flow units. In contrast to the other major flow units, the Cerberus Plains are composed of multiple lava flow-fields that are each generally smaller than the flood basalts infilling Grjótá Valles, Marte Vallis, and Athabasca Valles. The areal extent of all digitized flow-fields is shown in Figure 6. Based on the more detailed digitizing scale of 1:80,000, our results show that there are at least 19 separate flow-fields exposed at the surface (and three subsurface units) in addition to at least 18 Lava Shields composing the Cerberus Plains. Similar to lavas infilling Athabasca, Rahway Valles, and Marte Vallis, lava composing the Cerberus Plains is mostly fed by different segments along the Cerberus Fossae. However, lava units labeled 18 and 19 are likely not to be sourced by the Cerberus Fossae and instead could have been fed by fissures located in the southwest. Since the lava flow unit 19 was overprinted by younger lavas, specifically Athabasca Valles lavas in the west, the source region cannot be determined with certainty.

The stratigraphic relationships of the Cerberus Plains lavas are very complex and vary throughout the region. Generally, lavas forming the Cerberus Plains are overprinted by Athabasca Valles lavas and are thus older. Most Cerberus Plains lava flows are stratigraphically higher than the Marte Vallis lava flows, specifically lava flow unit 19 in the south, lava unit 9 in the north, and 8 in the west. However, lava units 6 and 18 seem to be stratigraphically lower than Marte Vallis lava and thus inferred to be older. Lava flow unit 17 forms the northern contact to Grjótá Valles and is stratigraphically higher and thus younger, the same is true for lava unit 5 that also partially buries the Rahway Valles lavas. Based on these observations, most lava flow units composing Cerberus Plains are part of the AEc$_3$ geologic unit from Tanaka et al. (2005). Some smaller units (e.g., lava flow 6 and 10) could be closer in age to the older part of the AEc$_3$ unit or even belong to the AEc$_2$ unit. However, to define age relationships of all flows, CSFDs would be required for all units, which would be challenging given secondary crater contamination from Zunil, Corinto, and Kota craters and is beyond the scope of this work. We further note that the Cerberus Plains do not show any rootless cones and thus it is unlikely that there was any lava–water/ice interaction during the time of the eruptions.

A few lava shields (tholi) are associated with Cerberus Fossae, but the majority of the tholi have vents that are not associated with the Cerberus Fossae and are spread throughout the region (Figures 3 and 6). The vents of the lava shields vary in shape from fissure-shaped to circular to elongated craters (Figure 11), even though the latter can be formed from an initial fissure that focuses into a more confined crater with an ongoing eruption. The vent morphologies of the lava shields often show similarities to small volcanic vents in other regions on Mars, such as the Tharsis Volcanic Province (Richardson et al., 2021). Most of the lava shields build a topographic relief, good examples can be found around 6.8°N and 159.8°E as well as 4.5°N and 158.8°E. The stratigraphic relationship of the lava shields and their surrounding lava flow-fields are very complex and vary throughout the region. The tholis do not show a trend that they are older than the surrounding lava flow-fields, instead the stratigraphic relationship between lava shields and surrounding lava flow-fields varies from location to location. The cluster of lava shields around 4.8°N and 169.5°E are embayed by Marte Vallis lavas and thus are older than the surrounding flood basalt. However, this cluster is stratigraphically younger than the Rahway Valles lavas in the north. The two very prominent and larger lava shields in the western part of Cerberus Plains also show different relationships to their surrounding lavas. The northern lava shield (6.8°N and 159.8°E) seems to be older than unit CP$_{14}$, which is in contact with the northern flanks and younger than CP$_{11}$ at its southern flanks. The southern lava shield (4.5°N and 158.8°E) is stratigraphically older than its surroundings (units CP$_{10}$ and CP$_{11}$), which is in agreement with the findings from Keszthelyi et al. (2021).

3.5. Athabasca Valles Lavas

Athabasca Valles lavas lie in the western part of the study site and cover a surface area of 257,195 km^2. This unit shares contacts with Grjótá Valles lavas in the north and the Cerberus Plains lavas in the east. Athabasca

Valles lavas are overprinting all units that this unit is in contact with and thus represent the youngest lava flow in Elysium Planitia, and on Mars in general, belonging to the AEc$_3$ geologic unit from Tanaka et al. (2005). Compared to other lava flow units in Elysium Planitia, the fissure that was feeding the Athabasca Valles lavas is easily traceable and is located around 10°N and 157°E, the most western segment of the Cerberus Fossae that was actively erupting lava. Jaeger et al. (2007, 2010) and Keszthelyi et al. (2021) provide detailed descriptions of the eruption and morphological characteristics of the Athabasca Valles lavas. The lava flow was moving toward the south into Athabasca Valles and split into two major branches relatively proximal to the vent: (a) moving toward the southeast into the Cerberus Plains; and (b) moving toward the southwest through a valley north of Aelis Planum and then flowing northwest, emplacing lava onto a plain close to the *InSight* landing site (Figure 3). The lava surface shows very pristine morphologies, and a transition of facies can be observed from proximal to distal flow parts. Close to the source fissures, several lava levels and overbank flows are exposed, indicating a non-steady state lava supply during the eruption. Athabasca Valles lavas share morphologies seen on other major flow units such as Marte Vallis, for example, disrupted crusts, including very well-defined lava plates. However, the prominent relationship of a peripheral of smooth, inflated crust associated with highly disrupted lava surfaces—which are very commonly observed in Marte Vallis and are interpreted to be late stage breakouts—are not typical throughout most of the Athabasca Valles lavas. While Athabasca Valles lavas generally created smooth continuous lava crusts at CTX-scale, the character is more similar to a thin lava veneer, likely as thin as a couple of decimeters at the flow margin (Figure 12), rather than inflated breakouts seen in Marte Vallis. While Athabasca Valles itself most likely has been carved by multiple episodes of aqueous activity, the observed surface morphologies are consistent with lava emplacement and do not require large amounts of water in the formation process. However, similar to other major flow units in Elysium Planitia, Athabasca Valles lavas have experienced lava–water or lava–ice interaction during the time of emplacement, as evidenced by numerous rootless cone populations throughout the region (Figure 3). The Athabasca Valles lavas show a dynamic interaction with the Medusae Fossae Formation, located along the southern contact of the lava flow-field. CTX and HiRISE data show that the lava is embaying the Medusae Fossae Formation in most locations. However, in a few cases (e.g., 3.8°N and 151.2°E) the lava seems stratigraphically lower than the Medusae Fossae Formation. Some individual lava surface features (e.g., plates, troughs, and ridges) can be traced across the surface despite being partially interrupted by overlying Medusae Fossae material. These observations support the hypothesis previously suggested by Kerber and Head (2010) and Keszthelyi et al. (2021) that parts of the reworked Medusae Fossae Formation are not only below, but also overlying the Athabasca Valles lavas, and the latter may represent reworked aeolian sediments or pyroclastic materials, which is younger than the lava emplacement itself.

4. SHARAD Investigation

To calculate the lava flow thicknesses of the flow units in Elysium Planitia, we investigated SHARAD reflectors in the late Amazonian volcanic unit (lAv; Tanaka, 2014). In a first step, we digitized all reflectors that do not correspond to surface clutter in the simulations. Analyzing the SHARAD tracks reveals that 462 out of 2,106 profiles contain at least one reflector. However, most of the profiles exhibit several reflectors summing up to a total number of 1,777 reflectors. Examples of typical reflectors for each major flow unit are shown in Figure 9 including examples for Grjótá Valles, Rahway Valles, Marte Vallis, Cerberus Plains, and Athabasca Valles. In addition, Figure 9 also shows examples for the Medusae Fossae Formation and Amazonis Planitia. When comparing the reflectors to the surface exposure of the geologic units, it becomes evident that the subsurface reflectors are well aligned with the geologic contacts seen on the surface. Prominent examples are located along the contact between lAv and the Hesperian and Noachian transition unit (HNt) in the southern as well as in the northern part of the Cerberus Plains (Figures 9 and 10e). Further alignment can be observed along the contact of lAv and the early Hesperian transition unit (eHt) at the western margin of the Athabasca Valles lavas in the Cerberus Plains and at the northwestern margin in Marte Vallis (Figure 10). Additionally, within the lAv unit, there are topographic steps visible in the subsurface SHARAD map (Figure 10) that are well aligned with flow margins. Good examples of these subsurface topographic steps are located at the Rahway Valles lavas boundary to Marte Vallis lavas at the northern and southern margin. Topographic steps are also visible in the lava flow units within the Cerberus Plains lavas which are overlapping the lavas infilling the proximal part of Marte Vallis, as well as between flow units CP$_9$ and CP$_{17}$ in the northern part of the Cerberus plains (Figure 10).

A region built of basaltic flows does not necessarily produce such a high density of radar reflectors, and the reasons for this have been discussed extensively in previous publications (e.g., Carter et al., 2009; Simon et al., 2014).

However, it is also likely that many interfaces in the subsurface are simply not visible in the SHARAD data either. At many locations where reflectors are interrupted, or where one would expect an interface based on surface geology, the radargram only shows a surface reflection. The underlying causes can vary and we will discuss the absence of reflectors below in the context of the individual units when it is affecting our interpretation. Nonetheless, in general terms, there are three possible causes for the absence of a reflector despite the presence of a subsurface interface. First, the reflectors may be too shallow and below the range resolution of SHARAD. Second, there is the possibility of an insufficient signal-to-noise ratio, resulting in a reflector being hidden beneath the noise floor of the instrument. This is most likely the case for deep reflectors and when the losses in the above material are high. Third, there may be a lack of a sufficient dielectric contrast between layers, which leads to a lack of an echo. This third reason makes the interpretation of layered reflectors particularly challenging as a reflector sandwiched between the surface and a deeper unit can appear in certain radargrams, but be absent in others. For this reason, a complete picture of the subsurface can only be obtained when considering the geologic context on the surface and evaluating the radargrams as an ensemble instead of looking at a few individual tracks in isolation.

To constrain the real part of the permittivity of the material of the individual units, we evaluated reflectors near the margins of mapped units that appear to pinch out to a flat surface, specifically within the lava flow units CP_9, Marte Vallis lavas, and Phlegra crater just north of the study site. We assumed that the elevation of the off-flow surface is the true elevation of the near-margin reflector and inverted for the corresponding permittivity. The results for the permittivity are based on 72 reflectors from the CP_9 unit. For the depth calculation of all reflectors we adopted the mean value of $\epsilon = 7.8 \pm 0.4$ (Figure 7). Permittivity values inverted from the other two units are consistent with this value; however, due to fewer reflectors at the distal part of Marte Vallis lavas and Phlegra crater there are larger uncertainties (compare to supplementary material).

The values inferred in this study are on the lower to middle end of the permittivities found by Carter et al. (2009) and Shoemaker et al. (2022) who investigated the properties of the flows west and northwest of Ascraeus Mons. Carter et al. (2009) found that the northern flow has permittivity values between 6.2 and 17.3, with an average of 12.2. For the southern flow, the authors found permittivity values of 7.0–14.0, with an average of 9.8. Northwest of Ascraeus Mons permittivity values are ranging from 7.0 to 11.2 (Shoemaker et al., 2022). The difference to the values found in the Tharsis region compared to our findings might be due to different lava densities pointing to higher porosities in the Elysium Planitia flows, which could be due to higher vesicularity and/or higher macroscale porosity between blocks of rubble. Other parameters that could affect the permittivity might be differences in mineral content and/or weathering as well as Fe and Ti oxides (Boivin et al., 2022; Stillman & Grimm, 2011; Stillman & Olhoeft, 2008).

Using the same empirical relation from Ulaby et al. (1988) that was also employed by Carter et al. (2009), we can derive the density ρ from the permittivity

$$\rho = \log \epsilon / 0.29, \tag{3}$$

which results in a bulk density of 3.08 ± 0.21 g/cm^3 in our study area. Assuming a grain density (excluding pore spaces) of 3.4 g/cm^3 for martian basalt (Baratoux et al., 2014; Carter et al., 2009; Kiefer et al., 2014), this would correspond to porosities ranging from 4% to 16% with a mean porosity of 9.53%. Note, however, that this equation assumes that the real part of the permittivity is only a function of density for dry material.

The average depths of the reflectors per unit are summarized in Table 1. The lava flow thicknesses range from a few meters to 104 m. More specifically, the thinnest lava flow detectable by SHARAD is 4.0 m, which is the distance of two SHARAD samples assuming a permittivity of 7.8, and the thickest lava has been observed in the Rahway Valles (RV) with 104 ± 6 m. Marte Vallis has the deepest detected reflector occurring at 140 m (keep in mind that Marte Vallis is home to several stacked reflectors and thus the deepest reflector is not equal to the thickest unit). Generally, the average thicknesses of the lavas composing Elysium Planitia range from 11 ± 5 to 28 ± 4 m (excluding the CP_{18} due to its uncertainty in origin, great depth, and segmented reflectors). The CP_{12} unit presents the lower end with an average thickness of 11 ± 5 m and the CP_{19} and Rahway Valles$_1$ (RV$_1$) units the higher end with average thicknesses of 28 ± 4 m and 27 ± 7 m, respectively (excluding CP_{18}). Amongst the major flow units in Elysium Planitia, Athabasca Valles lavas emplaced the thinnest average lava with 15 ± 6 m and RV$_1$ the thickest average lava. See Table 1 for the values of all units with reflectors present. We want to note, that very deep reflectors with no or little surface exposure and few reflectors spread throughout a larger

Table 1
Summary of Exposed Surface Areas (A_{exp}) Based on Our Geomorphological Map Combined With SHARAD Investigations: Areas (A), Average Thicknesses Based on SHARAD Reflectors (d_{avg}), Maximum Thicknesses (d_{max}), Calculated Volumes (V), and Related Dense Rock Equivalent (DRE) of All Flow Units in Elysium Planitia That Exhibit Reflectors As Well As Parts of Amazonis Planitia

Unit	A_{exp} (km^2)	A (km^2)	d_{avg} (m)	d_{max} (m)	V (km^3)	DRE (km^3)
AV	257,195	257,195	15 ± 6	79 ± 5	4,000 ± 1,600	3,700 ± 1,400
MV$_1$	491,767	579,454	21 ± 4	63 ± 4	12,200 ± 2,500	11,000 ± 2,300
MV$_S$	n/a	104,589	16 ± 6	75 ± 6	1,700 ± 600	1,500 ± 600
MV$_P$	n/a	71,632	12 ± 11	87 ± 13	900 ± 800	800 ± 800
RV$_1$	272,252	574,300	27 ± 7	104 ± 6	16,000 ± 4,000	14,000 ± 4,000
RV$_2$	n/a	392,652	22 ± 6	80 ± 6	9,000 ± 3,000	7,700 ± 2,600
GV	234,260	255,607	24 ± 13	56 ± 10	6,000 ± 3,000	5,400 ± 3,000
AP[a]	352,123	430,185	41 ± 11	100 ± 5	18,000 ± 5,000	16,000 ± 5,000
Cerberus Plains (measured)						
CP$_{10}$	28,718	50,966	16 ± 7	42 ± 3	800 ± 400	700 ± 300
CP$_{12}$	5,807	8,606	11 ± 5	32 ± 4	100 ± 50	90 ± 40
CP$_{13}$	4,434	10,706	23 ± 7	53 ± 5	250 ± 80	230 ± 70
CP$_{14}$	16,497	18,817	18 ± 6	35 ± 6	350 ± 120	310 ± 110
CP$_{19}$	126,644	132,895	28 ± 4	66 ± 4	3,700 ± 600	3,400 ± 600
CP$_{18}$	16,401	115,247	54 ± 7	68 ± 5	6,200 ± 800	5,600 ± 800
CP$_8$	6,613	6,613	19 ± 7	40 ± 10	160 ± 60	140 ± 50
CP$_6$	4,267	5,622	19 ± 4	31 ± 2	110 ± 20	100 ± 20
CP$_{17}$	54,623	70,155	25 ± 3	92 ± 12	1,700 ± 240	1,600 ± 240
CP$_9$	18,521	62,927	17 ± 8	56 ± 4	1,100 ± 500	1,000 ± 500
CP$_3$	5,007	47,208	23 ± 12	72 ± 11	1,100 ± 600	1,000 ± 600
Total[b]	271,131	414,515	n/a	n/a	9,400 ± 1,100	9,000 ± 1,000
Cerberus Plains (estimated)						
CP$_1$	722	n/a	23	n/a	17	15
CP$_2$	598	n/a	23	n/a	14	12
CP$_4$[c]	715	n/a	46	56	33	30
CP$_5$	21,977	n/a	23	n/a	500	460
CP$_7$	1,286	n/a	23	n/a	30	27
CP$_{11}$[c]	8,528	n/a	39	48	330	300
CP$_{15}$	2,536	n/a	23	n/a	58	53
CP$_{16}$[c]	375	n/a	19	n/a	7	6
Total	36,737	n/a	n/a	n/a	996	900
Shields (measured)						
LS$_1$	16,804	27,735	21 ± 5	45 ± 3	580 ± 130	530 ± 130
LS$_2$	10,225	16,346	35 ± 10	51 ± 10	570 ± 160	520 ± 150
LS$_3$	2,719	4,045	18 ± 5	23 ± 5	72 ± 21	65 ± 20
Total	29,748	48,126	n/a	n/a	1,221 ± 210	1,105 ± 200
Shields (estimated)						
LS$_4$	3,662	n/a	25	n/a	92	83
LS$_5$	3,619	n/a	25	n/a	90	82
LS$_6$	1,153	n/a	25	n/a	29	26
LS$_7$	4,000	n/a	25	n/a	100	90

Table 1
Continued

Unit	A_{exp} (km²)	A (km²)	d_{avg} (m)	d_{max} (m)	V (km³)	DRE (km³)
LS_8	312	n/a	25	n/a	8	7
LS_9	3,955	n/a	25	n/a	99	89
LS_{10}	502	n/a	25	n/a	13	11
LS_{11}	938	n/a	25	n/a	23	21
Total	18,121	n/a	n/a	n/a	454	410

Note. Please note, that very deep reflectors with no surface exposure and few reflectors spread throughout a larger area including Marte Vallis$_S$ and Marte Vallis$_P$ should be treated with caution.

[a]Note that this is just the area of Amazonis Planitia contained in our study area and not its total area. [b]Note, these values represent all the lava flow-fields in Cerberus Plains with reflectors except Lava Shields and CP_{18}. CP_{18} is excluded due to its uncertain nature, depth, and high error. [c]Units with less than two reflectors.

area (e.g., CP_{18}, Marte Vallis$_S$, and Marte Vallis$_P$) should be treated with caution. Best results were achieved with high reflector density and well-defined boundary conditions, for example, lava flows that were not or only partially covered by younger flows. For example, Athabasca Valles is the youngest flood basalt in Elysium Planitia, however, it has in some areas a relatively sparse abundance of SHARAD reflector and thus the uncertainty is relatively high. Marte Vallis has a high reflector density, is only partially covered and thus shows a low uncertainty (Table 1). Please see supplementary data for all calculated depth maps of the units and plotted SHARAD tracks with reflectors to indicate reflector density.

The radargrams for Amazonis Planitia, Grjótá Valles, and Athabasca Valles lavas typically show one vertical level of reflectors. Typical reflectors in Athabasca Valles are relatively shallow, a few tens of meters, with the deepest part located around 4.8°N and 151.5°E. The radargrams covering the proximal part of Athabasca Valles itself do not show any reflectors. Only once the lava exits the valley (∼300 km from the fissure), reflectors start to be visible. That is the case for both lava branches, entering the Cerberus Plains as well as the lava that flowed southwestward. Possible causes could be higher attenuation losses due to for example, surface roughness or the absence of a reflecting interface due to the erosion of the material producing the reflector or lava being emplaced in a more turbulent regime in the proximal part compared to the distal part. Further, since the lava was topographically confined, the flow velocities might have been much higher than downflow, where the lava entered a plain forming terrain. The same observations hold where the Athabasca Valles lava entered into a valley north of Aeolis Planum and only few reflectors are visible in the radargrams. In areas where the lava flow looks very thin in CTX and HiRISE images, for examples, the most distal extent or the lava lobes on the westerns side (6.8°N and 145.1°E), reflectors were not resolvable by SHARAD.

Radargrams covering Rahway Valles and Marte Vallis often show stacked reflectors (Figures 9b and 9c). These stacked reflectors are interpreted to represent the interface of different lava flow-fields. In Rahway Valles, there are two reflectors, continuously traceable in the northern portion of Rahway Valles. These two reflectors can be traced back all the way to Cerberus Plains and indicate, in combination with flow indicators of the surface, that Rahway Valles lavas were fed from Cerberus Fossae segments in Cerberus Plains. The shallower reflectors seem to be dipping toward the contact of Marte Vallis, whereas the deeper reflector is fading out earlier and does not show a direct interface to lavas occupying Marte Vallis. These two reflectors are interpreted to represent at least two lava flows plus the basement material or possibly three lava flow-fields infilling Rahway Valles. In addition to the morphological similarities, the depth of the reflectors south of the Marte Vallis lavas are similar to the reflectors in the northern portion of Rahway Valles. Thus, it is likely that these represent the interface of the same flow units and are consequently defined as Rahway Valles lavas. However, most radargrams in the southern portion only show one reflector that we interpret to be associated to the shallower unit in the northern part.

In the central region, where Marte Vallis is in contact with Rahways Valles, radargrams also contain several stacked reflectors. However, their relationship to one another seems more complicated than within Rahway Valles, which is evidenced by reflectors where the different horizons are not as easily traceable and distinguishable throughout the valley. In most locations, two reflectors are visible with strongly varying depths and shapes (Figure 9). In the central part of the Cerberus Plains (Figure 9) radargrams show a very prominent reflector that is

characterized by a strong and laterally extensive subsurface return signal. Mapping out the extent of this reflector shows that it creates the interface of the lava flow to what is likely the underlying RV_1 unit, thus representing a large but shallow buried valley system visible in the subsurface DTM (Figure 10). This western extent of Marte Vallis was previously detected by Xiong et al. (2021). However, the channel is much shallower than the authors suggested due to the fact that valley is infilled by lava (permittivity of 7.8) and not ice-rich material, which would have a permittivity of ∼3. Additionally, in MOLA and in the surface morphology we see evidence of lava inflation, which thickens the lava layer and can appear as a valley-shaped reflector in radargrams. When correcting for the surface topography using MOLA, the valley is much less prominent and the lava is mostly confined by the surrounding topography (e.g., lava shields and Hibes Montes in the north of the central valley and older Htu unit in the south).

The subsurface DTM as well as MOLA also indicate a topographic relief sloping down toward the southeast (Figure 10). If the MV_1 reflector is the interface of an aqueously carved channel or following the underlying topography, this would indicate a paleo-flow direction of the water from the northwest toward the southeast and would argue against the hypothesis that water was erupted from a now buried segment of the Cerberus Fossae (Morgan et al., 2013). Our morphological characterization of kinematic indicators on the lava surface shows that, from the location of the suggested buried Cerberus Fossae, the lava flow can be traced in an up-flow direction for over 1,000 km northwestwards, to an area with multiple vents in the northwestern part of Cerberus Plains. The flow is also not interrupted where the continuation of the Cerberus Fossae into the central part of Marte Vallis would be expected. Neither is the flow direction going in an opposite direction, away from the suggested buried Cerberus Fossae segment, which would have been expected if the lavas were fed from a buried southeastern extent of the Cerberus Fossae. Thus, we argue that the valley of Marte Vallis extends all the way northwestwards into the Cerberus Plains and we refer to the subsurface valley located in Cerberus Plains to as the "proximal portion" of Marte Vallis. Based on the combined surface and subsurface information we further argue that the lavas infilling the entire Marte Vallis system were fed from a Cerberus Fossae segment in the northwestern portion, just east of the fissure feeding the Athabasca Valles lavas. The most proximal part of Marte Vallis lava, however, is not exposed at the surface and instead appears to be buried by younger lobes from the Cerberus Plains lavas (see Figures 6 and 9c).

In the central Marte Vallis area, where Marte Vallis lavas are in contact with Rahway Valles lavas, the subsurface Marte Vallis reflectors show that the last lava emplaced is 20–40 m thick (e.g., embaying the kīpuka). These reflectors are also visible in previously published radargrams (Morgan et al., 2013). Due to the absence of reflectors in the underlying Rahways Valles unit in the southern part of central Marte Vallis, Morgan et al. (2013) suggested a deep (>80 m) buried channel. In this scenario (Figure 8a), aqueous erosion into RV_1 and RV_2 units carved a deep channel. This explanation is the most elegant interpretation and consistent with the surface observations, which was also favored by Voigt and Hamilton (2018). However, since the latest flow is only few tens of meters thick, an additional lava flow with a thickness of >50 m would have been needed to infill the deep channel within Marte Vallis valley. No surface exposure or other evidence is visible of such a voluminous flow unit. Further, if there was indeed a >80 m deep aqueous carved channel, then that would imply a large volume of eroded material, deposited in the downflow direction (such as in Amazonis Planitia), but no observations support a large sedimentary deposit associated with this channel system.

To overcome the challenge of the missing lava flow, a second hypothesis is that the RV_2 unit was emplaced (Figure 8b), and an aqueous process eroded into RV_2 forming the Marte Vallis channel. Subsequently, RV_1 lava was emplaced, infilling the previously carved channel. Major lava pathways of RV_1 were then drained (e.g., due to breakouts at the flow front or distal areas) mimicking the pre-existing topography. Kīpuka were eroded out of RV_2 material and the exposed surface of RV_1 simply inherited the underlying topography. Lava high-stands covering the islands remain preserved. Lastly, the MV_1 lava was emplaced onto RV_1. This hypothesis requires extensive lava drainage which is supported by geomorphological features such as bathtub rings (Voigt & Hamilton, 2018) observed in the same Rahway Valles basin.

Alternatively, multiple erosion events could also explain the present day surface and subsurface reflectors (Figure 8c). In this hypothesis, the RV_2 unit was emplaced, and an aqueous process eroded into RV_2 forming a channel. Subsequently, RV_1 lava was emplaced infilling the previously carved channel followed by a second erosion event carving a channel into RV_1 which was finally infilled by MV_1 lava. This scenario is consistent with previous interpretations of fluvial erosion arguing for Marte Vallis showing evidence for more than one flood (Burr et al., 2002).
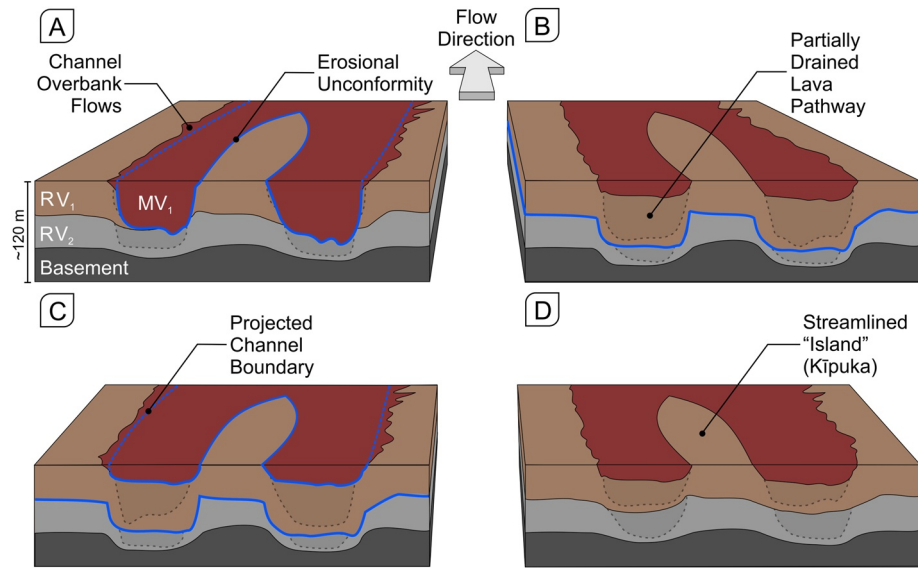
Figure 8. There are at least four scenarios how the central Marte Vallis area formed over time. (a) Subsequent emplacement of the RV_2 and RV_1 units over the basement material, followed by aqueous erosion (illustrated by the blue line) into the RV_2 and RV_1 units and infilling of the carved channel by MV_1 lava. (b) Emplacement of the RV_2 unit followed by an aqueous erosion forming a channel. The RV_1 unit infilled the channel and partially drained the main lava pathway (marked by the dashed line), followed by the emplacement of MV_1 lava. (c) Emplacement of RV_2 and a subsequent aqueous erosion event formed a channel. Emplacement of RV_1 followed by a second aqueous erosion event that was then infilled by MV_1 lava. (d) Emplacement of RV_2 and RV_1, both units partially drained in their lava pathways inheriting the pre-existing topography of the basement. Lastly, MV_1 lava was emplaced. No aqueous erosion event occurred after the emplacement of RV_2.

However, considering the layering of subsurface reflectors, it is also conceivable that no fluvial erosion was involved after the emplacement of RV_2 and RV_1. In this scenario (Figure 8d), the RV_2 unit was emplaced and was in filling pre-existing topography. Due to drainage events in distal areas, main pathways in Marte Vallis area drained mimicking the pre-existing topography (likely including a valley). RV_1 was emplaced and drained as well. Lastly, MV_1 lava was emplaced. In this case, the gaps in the RV_1 and RV_2 reflectors are due to the Marte Vallis lava shadowing the underlying units where the lava is thick.

The Cerberus Plains lavas are composed of several smaller lava flow-fields compared to the other major flow units that represent flood basalts. Most flow units contain strong and spatially continuous subsurface reflectors including flow units CP_{12}–CP_{14}, CP_8, CP_9, CP_{17}, and CP_{19} (cf. Figure 6 and Supporting Information S1). However, some of the individual flow-fields are lacking a subsurface return (e.g., flow units CP_5, CP_{11}, CP_{15}, and CP_{16}). The largest individual flow unit, CP_{19}, represents the thickest unit, while flows in the northwestern portion are the thinnest. The Cerberus Plains is also home to several lava shields. Most of the shield's basement material is not detected by SHARAD. However, three lava shields show SHARAD reflectors that we interpret to represent the base of the lava shields. For the DTM the cluster of lava shields in the east has been grouped into a single unit named $Shield_1$. The northern extent of the Cerberus Plains exhibits overlapping lava flow-fields (e.g., CP_9, CP_{17}, and MV_1 units in the east and CP_{11}, CP_{12}, CP_{13}, and CP_{14} in the west). There are at least two different scenarios how these overlapping flows are temporally related to one another and to their surroundings: (a) The overlapping lava flow-fields could represent a late stage during the same eruptive phase that produced the lowest stratigraphic unit (such as Marte Vallis lavas in the western example), or (b) the overlapping lava flow-fields could be formed as a results of different eruptions with significant time in between. Subsurface SHARAD reflectors indicate that the CP_9, CP_{17} as well as MV_1 represent flow fields are indeed formed by three separate eruptions. MV_1 lavas were emplaced first, followed by CP_9 lava field, and subsequently CP_{17}. The relationship between CP_{17} and CP_5 is less certain due to varying stratigraphic contracts along the flow margins and absence of SHARAD reflectors below CP_5. The overlapping flows in the west of Cerberus Plains all show subsurface reflectors indicating four different eruptions, with the oldest eruption emplacing lava flows belonging to CP_{11}, followed by CP_{12}, CP_{13}, and CP_{14}.

In addition to the lAv composing Elysium Planitia, this study also analyzed reflectors belonging to Amazonis Planitia located in the northeastern corner of the study site (Figure 3). These reflectors are consistently deeper
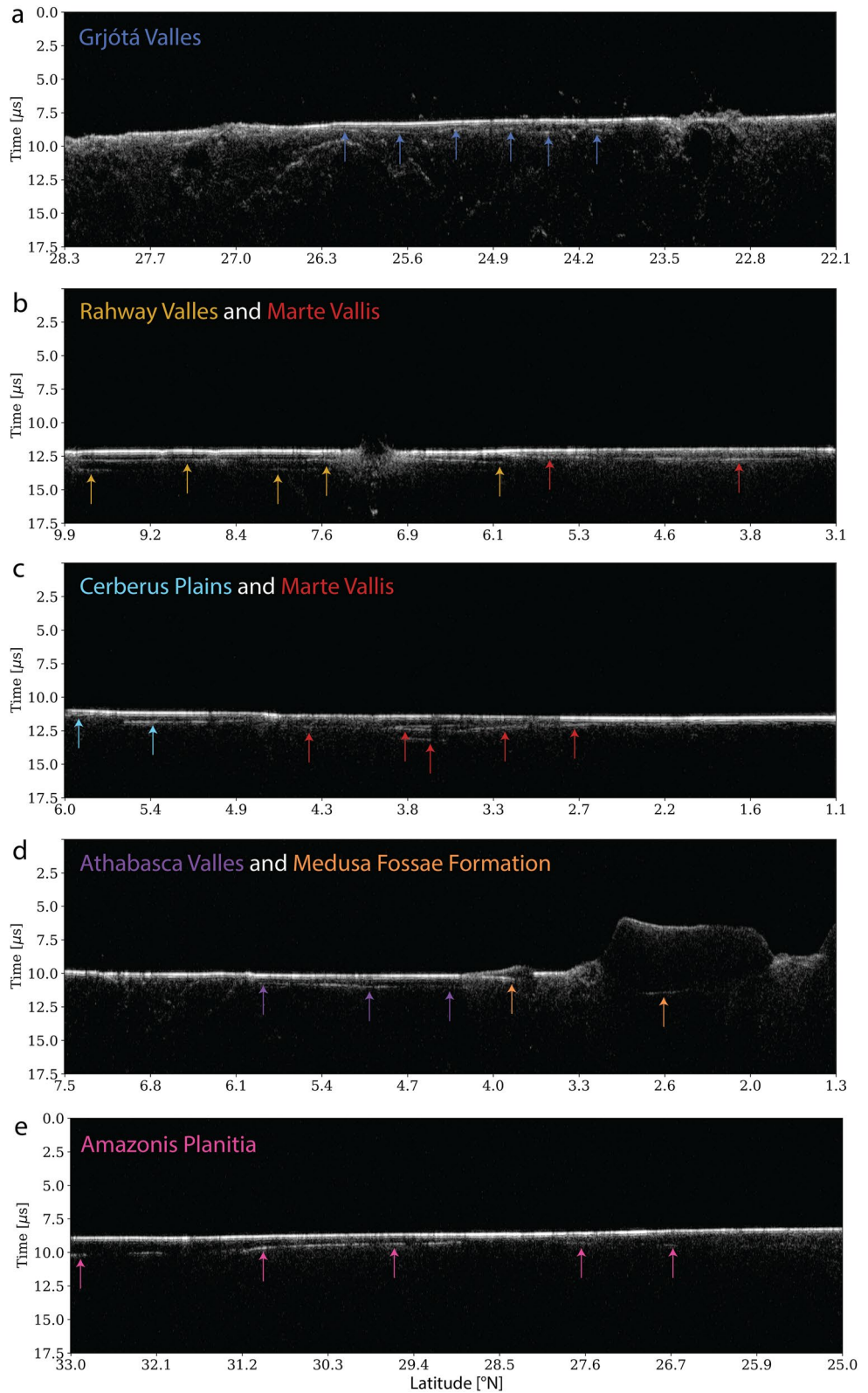
Figure 9. Examples of radargrams in Elysium Planitia including the main lava flow units: (a) Grjótá Valles, (b) Rahway Valles and Marte Vallis, (c) Cerberus Plains and Marte Vallis, and (d) Athabasca Valles and Medusae Fossae Formation; as well as (e) exposed lavas within Amazonis Planitia. Note several stacked reflectors in (b) Rahway Valles and (c) Marte Vallis.
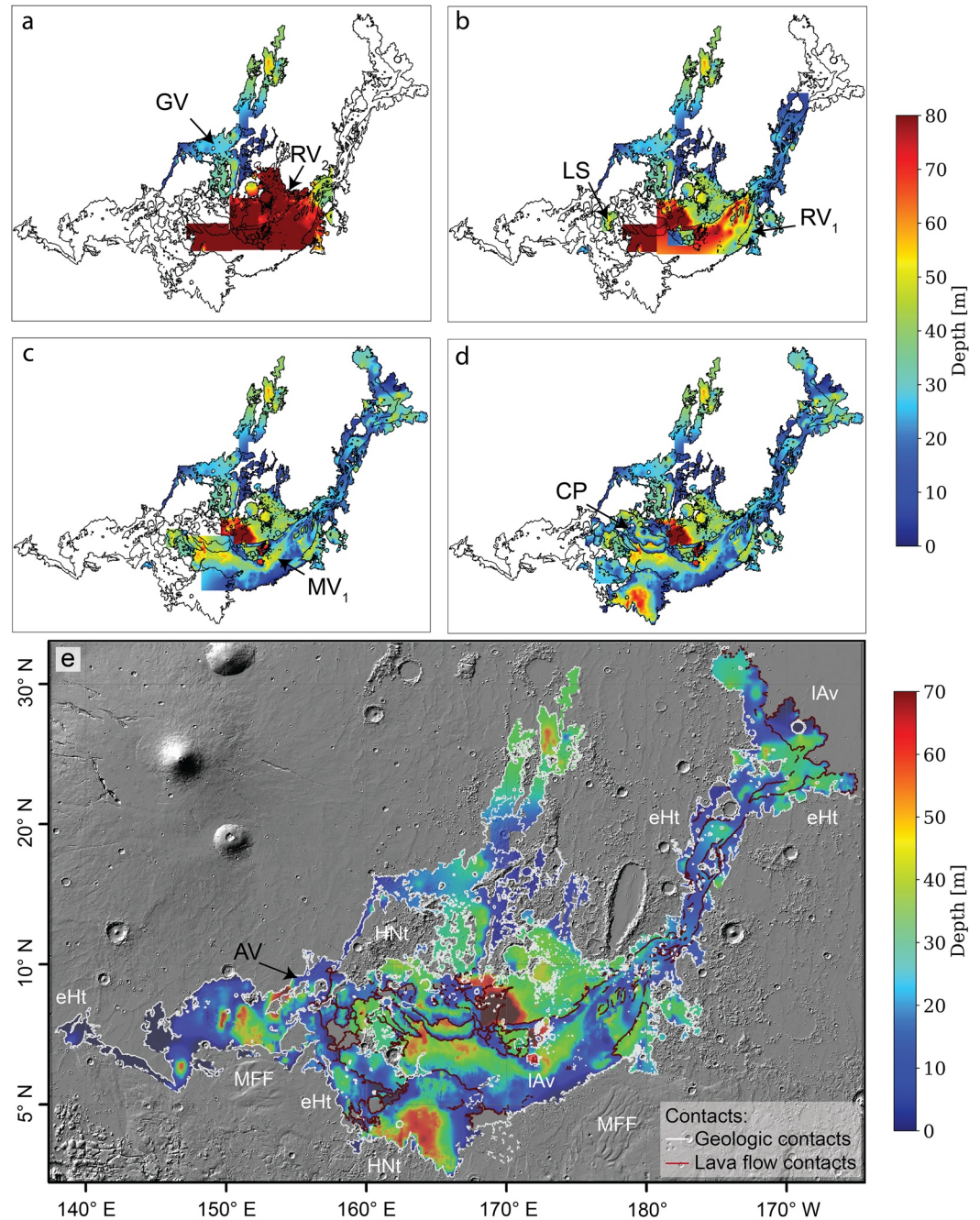
Figure 10. Color-coded depth maps constructed from the individual SHARAD reflectors and grouped into the five main lava flow units. (a) Emplacement of Grjótá Valles (GV) lava in the north and Rahway Valles 2 (RV_2) lava toward the south. (b) Emplacement of Rahway Valles 1 (RV_1) lava and Lava Shields (LS). (c) Emplacement of Marte Vallis 1 (MV_1) lava. (d) Emplacement of Cerberus Plains (CP) lava. (e) Emplacement of Athabasca Valles (AV) lava in the west and combined depth map of all upper units. The geologic boundaries (white lines) and flow margins (red lines) from our geomorphological mapping are shown in addition to the main geologic units that are in contact with the late Amazonian volcanic unit (lAv), including early Hesperian transition unit (eHt), Amazonian–Hesperian volcanic unit (AHv), Hesperian–Noachian transition unit (HNt), Medussae Fossae Formation (MFF). Note that the sharp edges in panel (a) and (b) are due to the interpolation limits of the respective units (see Section 2.2).

than the lavas in Elysium Planitia with an average thickness of 41 ± 11 m (Figure 9 and Table 1). Further, Amazonis Planitia lava thicknesses are less variable compared to Marte Vallis and Athabasca Valles lavas, as the lava was emplaced onto a plain rather than an aqueously carved valley system like in Marte Vallis and Athabasca
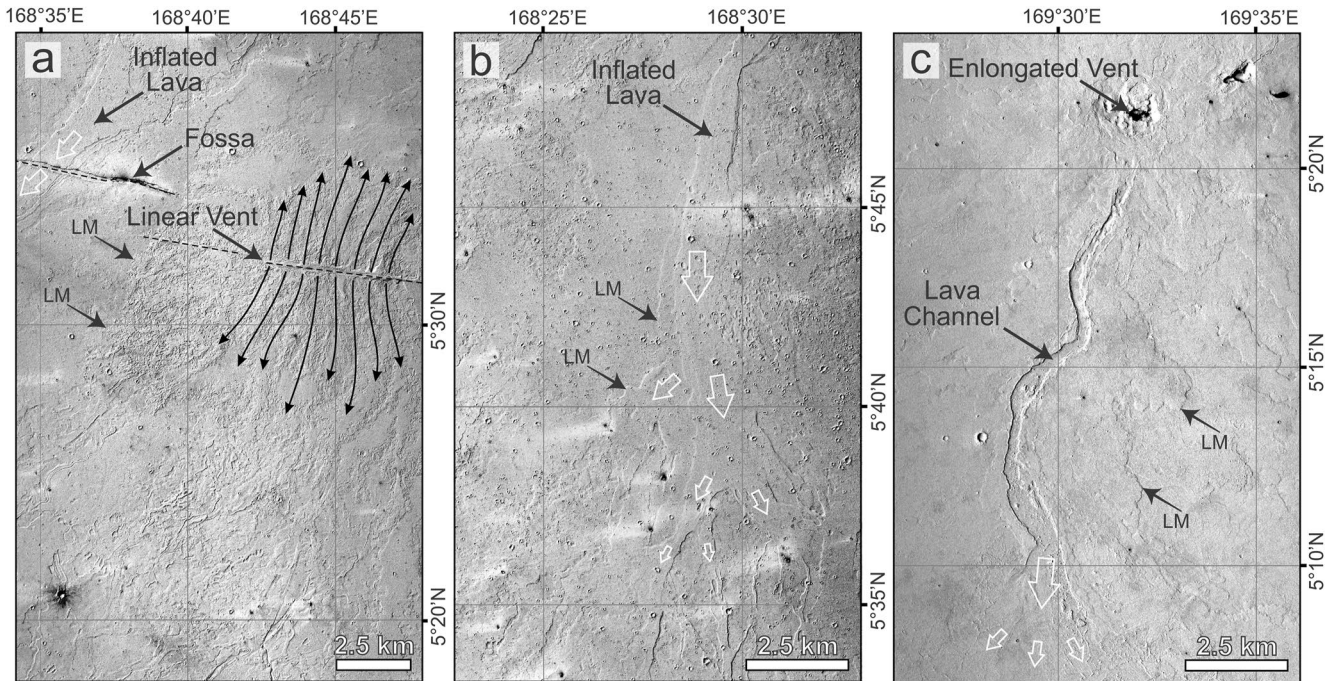
Figure 11. Typical morphologies of smaller lava flow-fields and lava shields in Cerberus Plains from CTX. (a) Inflated lava flows similar to pāhoehoe flow morphologies on Earth. Note, different cross-cutting relationships of Fosse and lava flow-fields. Fossae on the west is cutting previous emplaced inflated pathways, whereas the fissure on the east was feeding the lava flow-field empaced to the north and south (see black arrows). (b) Inflated pathways of the CP$_5$ unit with flow internal lobe margins (LM). (c) Confined vent into an elongated shape and narrow lava channel of a lava shield. Flow internal lobe margins (LM) are indicated as well.

Valles. Based on kinematic indicators and subsurface reflectors, it is likely that parts of the Amazonis Planitia lava exposed in our study site were emplaced in an east to west flow direction. This would imply that Amazonis Planitia lavas have a different magmatic feeder system than the lavas forming Elysium Planitia.

The deepest reflectors in the study area belong to the Medusae Fossae Formation, close to terrain that we interpret to represent reworked Medusae Fossae Formation fragments (see Figure 9d). However, the depth of these reflectors was calculated with a permittivity of 7.8, which is likely too high for materials forming Medusae Fossae Formation and its reworked material. Considering previous estimates of the real dielectric constant of 2–3 in the Medusae Fossae Formation (Campbell et al., 2021; Carter et al., 2009; Watters et al., 2007), the depths are likely underestimated in this study.

5. Lava Volumes

Combining the surface information of our mapping with the subsurface information of our SHARAD analysis, we can constrain the erupted lava volumes of the flow units composing Elysium Planitia. Lava flow depths have been calculated from the reflector depth map (Figure 10 and Supporting Information S1) and integrated over the area of each respective unit. Volumes are presented in Table 1 with two different distinctions based on the method. Measured lava volumes include lava flow-fields that contain enough subsurface reflectors to calculate the volumes. These volumes are considered more accurate and also include uncertainties. In contrast, estimated lava volumes include flow-fields that only have two or less reflectors. In these cases, the exposed area in combination with the average thickness of the few reflectors or average thickness in Cerberus Plains/Lava Shield group was used to estimate the volume. In cases with no or few reflectors, the volume should be treated with caution because they are derived with an estimated thickness. For simplicity, we start by discussing the lava volumes of the major flow units. Note that Cerberus Plains lava are composed of several lava flow-fields and are grouped together in the first part of the description.

Athabasca Valles lavas represent the smallest flow unit of the five major flow units with an erupted volume of 4,000 ± 1,600 km^3. Assuming a porosity of 9.5% ± 5% as derived from a permittivity of 7.8, the Dense
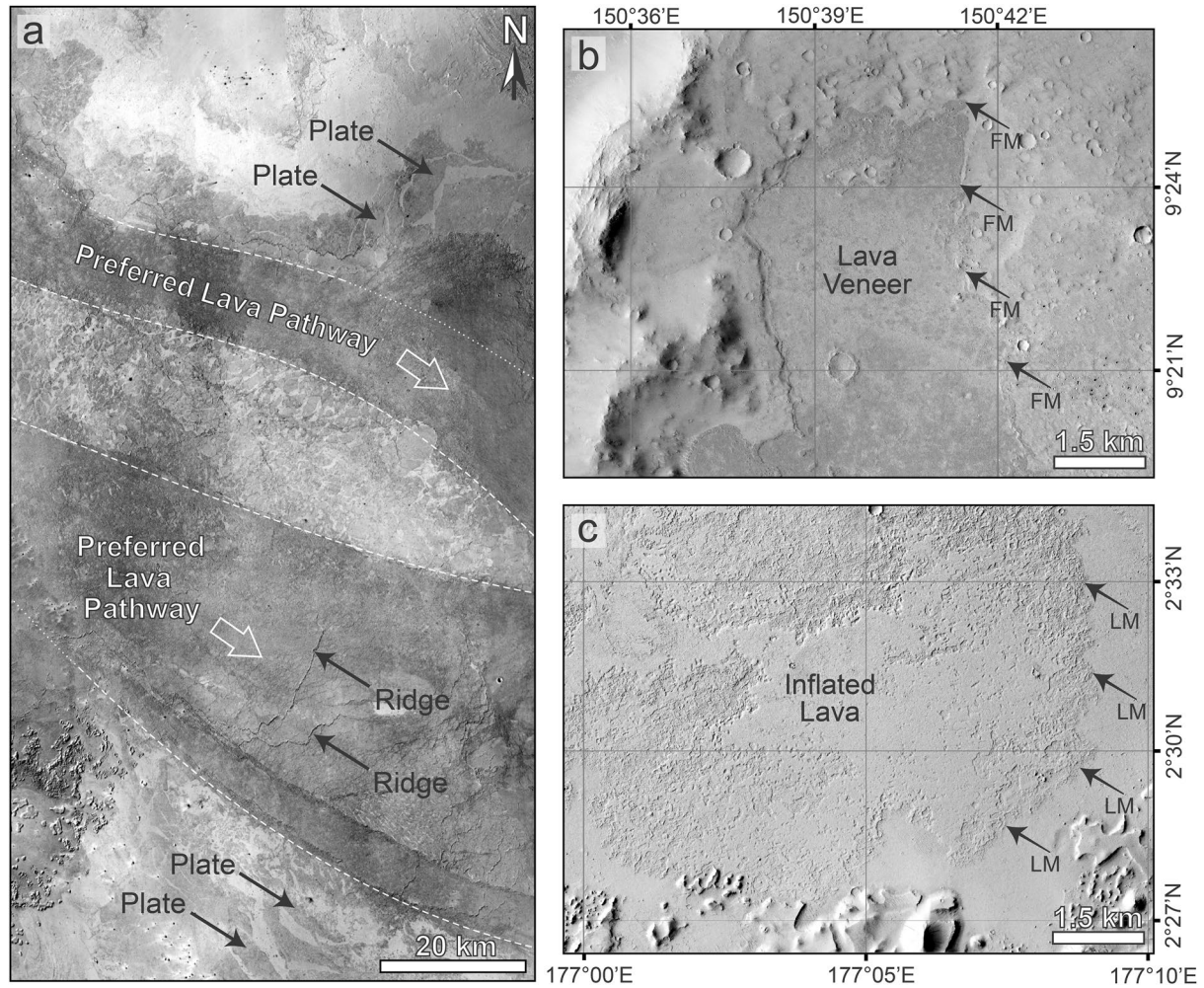
Figure 12. Examples of pristine flood lava surfaces from the Athabasca Valles and Marte Vallis lavas. (a) View across the Marte Vallis in the Cerberus Plains region (CTX mosaic from Dickson et al. (2023) is centered on 169°86′E and 2°78′N). The low albedo regions represent highly disrupted lava crusts exhibiting ridges and plates of the channel. (b) Examples Athabasca Valles of flow margin (FM) with very thin lava as seen by CTX. (c) Examples of typical Marte Vallis lobate margins (LM) with inflation features (CTX). Note different characteristics at the same scale of Athabasca Valles (b) and Marte Vallis (c) lavas.

Rock Equivalent (DRE) is $3,700 \pm 1,400$ km³. The determined volume is in agreement, but on the lower end, with previous estimates by Jaeger et al. (2010), where the authors concluded that Athabasca Valles had erupted 5,000–7,500 km³ of mafic or ultramafic lavas based on a similar surface area. Jaeger et al. (2010) observed that the exposed lava thicknesses are all rather shallow and therefore concluded that a reasonable thickness is about 20 m. Our investigations show that Athabasca Valles has an average thickness of 15 ± 6 m, which is an average slightly thinner than the previous estimates. However, our analysis of SHARAD reflectors shows that the flow thickness is locally significantly higher than 15 m, with lava flows up to 79 ± 5 m thick.

Grjótá Valles lavas in the northern part of Elysium Planitia is the second smallest unit of the five major flow units with a volume of $6,000 \pm 3,000$ km³ and a DRE of $5,400 \pm 3,000$ km³. The large formal error in this unit is due to the sparse radar reflector coverage. However, the volume should be treated as a minimum, mainly because the southern boundary/extent of this unit is hard to constrain. While we do not see SHARAD reflectors going into Rahway Valles and Cerberus Plains which could be easily defined as Grjótá Valles reflectors, the absence of reflectors in these regions might not necessarily define the southern contact. Additionally, lava flows in Cerberus Plains are younger than Grjótá Valles lavas and thus overlay the most southern extent. The average thickness of the surficial unit in Grjótá Valles is 24 ± 13 m. The maximum depth we found was 56 ± 10 m, which is slightly shallower than previously reported maximum lava thickness of 80 m in the most northern extent of the Grjótá Valles lavas unit (Hamilton et al., 2010, 2011), which were estimated based on MOLA profiles. However, based

on our geomorphological observations, the northern extent has a different character than areas closer to the vent. Specifically, the most northern extent and the focus of the study in Hamilton et al. (2010) has experienced intense inflation and represents in average a much thicker lava flow unit than other parts within Grjótá Valles (e.g., thin veneers close to the fossae).

When combing all lava flow-fields in the Cerberus Plains, the unit represents the third largest major flow unit with an erupted combined volume of $9,400 \pm 1,100$ km^3. However, this number does not account for all nineteen flow-fields as only 11 of these units have a sufficient amount of reflectors to calculate a volume. The result should therefore be considered as a lower boundary. Combining the exposed area with an average thickness shows that the remaining lava flow-fields have an estimated volume of 996 km^3 and thus they likely represent less than ~10% of the actually measured volumes. Additionally, the CP_{18} unit is excluded from this lava volume due to its uncertain nature, great depth, and high error. A list of all flow units composing the Cerberus Plains with areas, average thicknesses, and volumes is provided in Table 1.

The second largest volume is observed in Marte Vallis with $12,200 \pm 2,500$ km^3 or a DRE of $11,000 \pm 2,300$ km^3. Marte Vallis is characterized by stacked reflectors and the reported volumes represent the upper most unit and thus the latest eruption. All Marte Vallis units together are $14,800 \pm 2,700$ km^3 in volume. The most recent lava infilling Marte Vallis has an average thickness of 22 ± 5 m with a maximum thickness of 63 ± 4 m. In total we identified five different horizons that are located in, and infilling, the Marte Vallis valley, labeled Marte Vallis$_1$, Marte Vallis$_S$, Marte Vallis$_P$, and then the underlying Rahway Valles$_1$, and Rahway Valles$_2$ units. Marte Vallis$_1$ is the last eruption event and the unit exposed at the surface in the Marte Vallis valley. Marte Vallis$_S$ and Marte Vallis$_P$ are units that are not exposed to the surface and located in the western part of the Marte Vallis valley close to the source region. Prior the emplacement of the Marte Vallis$_1$ unit the valley was occupied by Rahway Valles$_1$ lavas that are exposed to the surface in the north in Rahway Valles and a southern portion, as well as exposed kīpuka, in the central part of Marte Vallis. We also identified deep reflectors belonging to the Rahway Valles$_2$ unit, however this unit is not exposed to the surface.

The largest major flow unit in Elysium Planitia is Rahway Valles$_1$ lavas, with a volume of the surficial material of $16,000 \pm 4,000$ km^3. The average thickness of the upper lava flow is 27 ± 7 m. Rahway Valles lavas have two layers of reflectors, Rahways Valles$_1$ and Rahways Valles$_2$. These two units combined give a total volume of $25,000 \pm 5,000$ km^3, which is larger than Marte Vallis lavas combined, however the uncertainty in Rahway Valles is higher. Rahways Valles$_1$ is exposed to the surface whereas Rahways Valles$_2$ is covered. Both units continue through the Marte Vallis valley with kīpuka surface exposures of Rahways Valles$_1$ and south at the contact to the older highlands. The average thicknesses, areas, estimated volumes, and DREs of all major units are summarized in Table 1.

6. Discussion

The origin of the surficial flow units within Elysium Planitia has been the subject of a long-standing debate. Proposed flow materials in Elysium Planitia include lava (e.g., Jaeger et al., 2007, 2010; Keszthelyi et al., 2004; Vaucher, Baratoux, Mangold, et al., 2009; Voigt & Hamilton, 2018), ice (e.g., Murray et al., 2005; Xiong et al., 2021), and periglacial deposits (e.g., Balme & Gallagher, 2009; Ramsdale et al., 2015). Findings in support of volatile-rich materials on the surface or subsurface include morphological observations of fluvial features and large outflow channels (e.g., Burr & McEwen, 2000; Burr et al., 2002), a few terraced craters, locally exposed ice in crater ejecta of a recent impactor (on 24 December 2021; Posiolova et al., 2022), volcanic rootless cones (VRCs; Fagents & Thordarson, 2007; Fagents et al., 2002; Frey, 1987; Hamilton et al., 2010; Lanagan et al., 2001; Noguchi & Kurita, 2015), as well as low permittivities in the Cerberus Plains (Xiong et al., 2021). The following sections discuss: (a) the origin of the surface material (i.e., the role of lava vs. ice); (b) possible sources for water; (c) emplacement styles; and (d) lava volumes and relative estimates on effusion rates.

6.1. The Role of Lava Versus Ice

There have been two recent papers by Xiong et al. (2021) and Harish et al. (2023) discussing the material properties in Elysium Planitia analyzed by SHARAD. Xiong et al. (2021) used HiRISE DTMs of impact crater terraces in Elysium Planitia to identify possible subsurface interfaces that may correspond to SHARAD reflectors and derive the bulk real permittivity, which they estimated to be 3.12, suggesting the possible presence of subsurface

water ice. However, terraces found within impact craters do not necessarily correspond to subsurface dielectric interfaces detected by SHARAD, and the uncertainty associated with those estimates was not provided.

Harish et al. (2023) followed a similar approach based on HiRISE DTMs of visible layering exposed along Cerberus Fossae, finding three main units: a 3–5 m thick regolith cover, a ~30 m thick layered unit, and ~260 m thick bouldery unit. They hypothesized that the stratigraphic boundary between the second and the third unit at ~34 m depth corresponds to a dielectric interface capable of generating reflectors detected in SHARAD profiles across Cerberus Fossae, estimating a bulk real permittivity of 9.34 ± 1.01 (at 1σ), in turn suggesting the presence of thick, dense shergottite-type basaltic material along the Cerberus Fossae. Harish et al. (2023) also calculated the loss tangent of the same materials following the methods of Campbell et al. (2008), obtaining a mean loss tangent of 0.027 ± 0.01, which is at least an order of magnitude higher than that of water ice found elsewhere on Mars (e.g., Petersen et al., 2018) and is compatible with basaltic lava flows (e.g., Morgan et al., 2015).

Our geomorphologic mapping reveals that all surfaces exhibit features consistent with lava flow emplacement, including lobate margins, inflation plateaus and pits, and "platy ridged" terrains. Moreover, our investigations of the dielectric properties using SHARAD data give values consistent with basalt, but are not compatible with water or ice. Therefore, our results show that the latest materials forming Elysium Planitia are dominated by lava flow-fields formed by effusive eruptions and do not support the interpretation that the large valleys are filled by ice-rice sediment or pure ice (e.g., Murray et al., 2005; Xiong et al., 2021). However, the recent impact crater in Amazonis Planitia just north of our study site (impactor excavated ice at 35°N; Posiolova et al., 2022) shows that it is possible to have some local ice patches in the near subsurface also at low latitudes. This conclusion is supported by the presence of terraced craters (a total of five found in this study) that might suggests the presence of ice during the time of impact. Additionally, the presence of VRCs indicates that lava interacted with volatile rich sediment during the time of some eruptions that occurred in Elysium Planitia (e.g., AV, GV, and most distal end of MV lavas see Figure 3 for locations). The thickness of a lava flow is roughly equal to the maximum depth that a thermal pulse could penetrate into the substrate on Mars and volatize ground-ice before the core of the lava flow solidifies (Fuller & Head, 2002; Hamilton et al., 2010). Therefore, the formation of VRCs by processes of molten–fuel coolant interaction implies the presence of a shallow volatile-bearing layer within the substrate. VRCs in Athabasca Valles mainly occur in locations with thin (~20-m-thick) lava, but also occur within a lava-filled basin north of Aeolis Planum, where lava thickness reach up to about 60 m. In Grjótá Vallis, lava flow thickness with VRC populations are commonly 30–55 m and in Marte Vallis associated lavas are 30–45 m thick. This indicates that water, in the form of wet sediments and/or ground ice, must have been present in near-surface within the first tens of meters at the time of lava flow emplacement. This would have represented a fundamentally different source of water than a global deep-aquifer reservoir (Clifford et al., 2000; Palumbo & Head, 2020), but it is unclear whether the H_2O sourced from a flooding event that proceeded lava emplacement, obliquity-driven climate change leading to the emplacement of low-latitude ground-ice, deposition by snow, or emplacement of localized ice deposits in association with volcanogenic volatiles that were released into the atmosphere. Therefore, we argue that while the bulk of the material forming Elysium Planitia consists of lava flows, local ice deposits near the surface were almost certainly present in the past and might still persist today.

Furthermore, our findings are consistent with results from the *InSight* mission, Wright et al. (2022) investigated the shallow subsurface in regard of cementation beneath the landing site. Their work showed that within the first 300 m no ground-ice or liquid water-saturated layers are likely to exist to date, however, it might be possible for fractured basalt with pores spaces to contain up to 20% ice. Additionally, if a ice-saturated layer would be present in Elysium Planitia, it would need to lie in between ~100 m (based on our SHARAD results) or 300 m (Wright et al., 2022) and 8 km (Manga & Wright, 2021).

6.2. Potential Sources of Water

The widespread distribution of VRCs within Elysium Planitia (Figure 3) implies explosive lava–water interactions involving molten lava and near-surface water or ground-ice deposits (Fagents & Thordarson, 2007; Fagents et al., 2002; Frey, 1987; Hamilton et al., 2010, 2011, 2017; Lanagan et al., 2001). If the probability of VRC distribution within flood basalt units was primarily a function of latitude, then the most likely source of the ice would be vapor diffusion under conditions of high obliquity (Fastook et al., 2011; Forget et al., 2006; Head & Marchant, 2003). However, the occurrence of VRCs close to the equator (i.e., within the geologically recent Athabasca Valles Flood lava) is difficult to reconcile with the relatively low obliquity modeled for Mars during the past 5 Ma (Laskar et al., 2004).

An alternative explanation for the origin of water or ice in the region could be the release of groundwater via the eruption of aqueous floods onto the surface immediately prior to lava emplacement. Floodwater would be expected to concentrate within confined valleys, topographic basins, and the termini of outflow channels. In general, this is where VRCs occur within Elysium Planitia, which suggests that megafloods may serve as the primary source of water and/or ice involved in explosive lava–water interactions and VRC formation (Burr et al., 2002, 2005, 2009; Fuller & Head, 2002; Plescia, 2003).

Nonetheless, under a variety of obliquity and dust opacity conditions, climate models predict that snow and ice accumulation can occur in parts of Elysium Planitia (Madeleine et al., 2009), including the northeastern parts of the Cerberus Fossae 2 unit (AEc_2) forming Grjótá Valles lavas, which include numerous VRC groups (Hamilton et al., 2010, 2011). Snow accumulation could also explain the presence of other lava–ice interactions such as the formation of topographic depressions formed between inflated lava flow margins and former topographic obstacles, which are interpreted as evidence of former snow/ice-bearing lobate debris aprons (Hauber et al., 2008).

A final possibility is that large volcanic eruptions could have significantly affected water and other volatile abundances in the atmosphere. There is no evidence to support that geologically recent flood basalt eruptions in Elysium Planitia triggered global climate changes and widespread surface water runoff events during the Late Amazonian (Baker & Head, 2015; Carr, 2007), but water released into the atmosphere may have been deposited on (or near) the surface as snow or ice (Hamid et al., 2023). These local ice deposits could have been volatilized by subsequent lava flow emplacement, gradually sublimating back into the atmosphere after the end of the eruption, or been protected by the co-emplacement of ash or other sedimentary deposits (Wilson & Head, 2009).

Assuming 0.5–1.8 wt% H_2O in the parent magma for the massive lava flows erupted in Elysium Planitia (based on shergottites, nakhlites, chassignites (SNC) meteorite compositions; Filiberto et al., 2016; Karlsson et al., 1992; McCoy et al., 2011; McSween et al., 2001), we can infer the total amount of water released into the atmosphere. Using our measured total volume of $95,000 \pm 9,000$ km^3 and the derived density of 3.08 ± 0.21, the combined eruptions within Elysium Planitia would have released 1 to 6×10^{12} kg of H_2O. In the present day, weakly oxidizing atmosphere of Mars, volcanic gases such as H_2O, CO_2, and SO_2 are expected to dominate volcanic emissions, along with smaller amounts of H_2S, HCl, HF, and other trace gases. H_2O emitted by volcanoes is an area of active research (Hamid et al., 2023; Kerber et al., 2011; Paladino et al., 2023). On Earth, H_2O emitted by volcanoes ($\sim 1.11 \times 10^{12}$ kg/year, counting both arc-volcanics and mid-ocean ridge basalts; Fischer, 2008) is often neglected, as it represents a negligible amount of water with respect to the total amount of water in the atmosphere at any given time ($\sim 1.46 \times 10^{16}$ kg; Gleick, 1996). However, on Mars, the amount of water in the atmosphere is about 10,000 times smaller ($\sim 1.45 \times 10^{12}$; Feldman et al., 2004), and therefore the eruption of volcanic water in the inferred amount can have a much larger effect. Thermal modeling of volcanism in Elysium Planitia has suggested possible lava effusion rates up to 10^6 m^3/s (Keszthelyi et al., 2000). Assuming a water content of 1.8% (McSween et al., 2001), this would translate to a water vapor output rate of 1.8×10^7 kg/s. However, these effusion rates do not seem consistent with the here inferred volumes as it would require Elysium Planitia to be formed in a single day. Nonetheless, atmospheric water content could have abruptly increased on Mars from volcanic eruptions, and this amount of water could potentially overwhelm the atmosphere's holding capacity and could lead to ice deposition at locations that would otherwise be out of equilibrium with the currently stable ice deposits.

The presence of mid- to low-latitude ice exposed within fresh impact craters in parts of Amazonis Planitia (Posiolova et al., 2022) suggests that ice is stable outside the region expected for obliquity-controlled ice deposits (Fastook et al., 2011; Forget et al., 2006; Head & Marchant, 2003) and snowfall (Madeleine et al., 2009). This may imply the preservation of ice associated with megaflood deposits or volcanogenic volatiles that were preserved beneath a layer of sediment, but given the concentration of VRCs within outflow channels, water concentration within megaflood corridors provides the most reasonable explanation for the origin of the water and ice during the time of eruption.

6.3. Emplacement Styles

In Elysium Planitia, we observe various lava morphologies indicating different emplacement styles throughout the area. Generally, it seems that smaller volume lava flow-fields—e.g., CP_5 close to Cerberus Fossae (Figures 11a and 11b) and lava shields (Figure 11c)—have morphologies similar to pāhoehoe lava on Earth. Close to their vents (e.g., segments of the Cerberus Fossae) the flows often show channelized flows (Figure 11c) and evidence of inflation along the pathway as well as in the distal end, including lava rise pits and plateaus (Figures 11a–11c).

In contrast, the most pristine flood basalts infilling the large valley systems (e.g., Athabasca Valles and Marte Vallis) show vast areas of highly disrupted lava crusts, including plates and ridges, wakes, and islands (Figure 12a). However, even amongst Athabasca Valles and Marte Vallis lavas we see differences in morphologies which are likely linked to their respective emplacement dynamics. Compared to Marte Vallis, the morphologies within Athabasca Valles indicate very little inflation, which is evidenced by the relatively shallow thickness of the lava lobes (as thin as a few decimeters; Figure 12b) as well as smaller sizes of the pits and plateaus. Instead, inflation within Athabasca Valles is confined to the most distal areas in the western extent and along a few distal flow margins in the eastern branch. This observation implies a relatively short emplacement time (Jaeger et al., 2010). In comparison, the Marte Vallis lavas show morphological evidence for inflation on almost all flow margins, and the Marte Vallis lavas have formed large lava lobes/flow-fields with intense inflation features (e.g., southern extent of central Marte Vallis; e.g., Figure 12c). In Marte Vallis, we also observe inflation characteristics within the highly disrupted crusts. Inflation of disrupted lava surfaces was previously reported within rubbly lavas in Iceland (Voigt, Hamilton, Scheidt, et al., 2021), indicating that the morphologies in Marte Vallis are likely representing rubbly lava rather than 'a'ā flows. Additionally, there is a strong spatial relationship between the highly disrupted lava surface (e.g., "rough undifferentiated" and "rough knobby" facies; Voigt & Hamilton, 2018) and the smoother more continuous lava surface (e.g., "smooth lobate pitted plateau" and "smooth lobate pitted irregular" facies; Voigt & Hamilton, 2018). This relationship indicates that the continuous lava facies forms as breakouts from the disrupted lava unit (e.g., rubbly facies; Figures 4a and 4c) and might only form as a secondary squeeze out rather than a standalone lava facies. Furthermore, at the 2014–2015 Holuhraun eruption in the highlands of Iceland this relationship of spiny breakouts sourced from a previously emplaced core with a rubbly crust was correlated with a decrease in local effusion rate (Voigt et al., 2022). Since we see much larger areas with inflated lava crust in Marte Vallis lavas than in Athabasca Valles, we suggest that lavas infilling Marte Vallis had smaller (but still very high) effusion rates and a longer eruption duration than lavas infilling Athabasca Valles.

The morphological differences within Marte Vallis lavas also suggest varying local effusion rates. Where lavas infilling the deeper parts of Marte Vallis formed disrupted lava crusts, indicative of relatively high effusion rates and potentially pulsating in the lava supply. In contrast, lava surfaces associated with shallower depth (e.g., embaying plains at the southern extent of Marte Vallis) show continuous crusts and lava inflation characteristics likely representing late-stage breakouts with a low local effusion rate and a more continuous lava supply (Figure 12b). In addition to the high voluminous flood basalts, Elysium Planitia and specifically Cerberus Plains is home to several smaller volume lava flow-fields. The different scales of lava features, such as their pathway—e.g., well confined narrow lava channels forming lava shields (Figure 11c) compared to ~100-km-wide lava pathways in Marte Vallis (Figure 12a)—imply vastly different eruption conditions such as effusion rates. The decreasing flow distances from the vent regions of these lava flow-fields, two order of magnitude scale difference of lava pathways, and overall smaller erupted volumes might imply an overall smaller effusion rate for some lava fields in Cerberus Plains and lava shields as well as a shorter eruption duration compared to the Marte Vallis flood lava. In addition to the lava emplacement, there seems to be a general difference in the style of water release and erosion in Elysium Planitia. The older Rahway Valles and Grjótá Valles regions show features consistent with a more continuous water release forming fluvial channel systems. Whereas the younger Marte Vallis and Athabasca Valles show morphologies indicative of a catastrophic high voluminous aqueous carving events.

6.4. Lava Volumes and Estimates on Effusion Rates

It is important to emphasize that our findings show that Elysium Planitia is composed of materials from multiple eruption events. The volcanic eruptions were spread throughout time and area. Even the large valley systems (e.g., Marte Vallis and Rahway Valles) show multiple eruption periods and thus do not reflect a single, extensive lava emplacement event. Our results show that the main volcanic activities were focused around ~125 Ma in Grjótá Valles (Hamilton et al., 2010), 20 Ma in Rahway Valles (Voigt & Hamilton, 2018), 9 Ma in Marte Vallis (Voigt & Hamilton, 2018), and 2.5–20 Ma in Athabasca Valles (Golder et al., 2020; McEwen et al., 2005; Murray et al., 2005; Vaucher, Baratoux, Toplis, et al., 2009), producing high volume flood basalts. However, our results do not indicate a singular direction for dike propagation. Instead, the activity along Cerberus Fossae segments exhibited back-and-forth movement over time. In Grjótá Valles, the source propagating was observed to be eastwards with time and was interpreted to be due to an eastward motion of the dike causing water release (Brown & Roberts, 2023). However, that general trend observed in Grjótá Valles is inconsistent with our findings in the entire Elysium Planitia area. For example, Marte Vallis lavas were fed from a western segment of the Cerberus

Fossae and the younger overlapping lavas were fed from segments moving toward the east with time. Lastly, the youngest Athabasca Valles lava was then fed from the most western extent of active vents. Thus, our findings suggests that there is no clear trend of dike propagation in one direction and instead the active vents rather moved around with time. In addition, the central part of Elysium Planitia, Cerberus Plains, which is home to most of the source regions, shows evidence of very complex lava flow-fields with most products having smaller volumes, but still large volumes compared to the other major lava units (GV, RV, MV, and AV). On Earth, the lava flow-fields in Cerberus Plains would still be classified as flood basalts since they have volumes larger than 100 km^3, however most of them are an order of magnitude smaller than the major flow units. Also, based on stratigraphic relationships, these lava flow-fields are ranging in time (~125 to 2.5 Ma). This finding is based on our geomorphological mapping, previously published ages from CSFDs (e.g., Hamilton et al., 2010; Jaeger et al., 2010; Voigt & Hamilton, 2018), as well as the fact that we see SHARAD reflectors of the different units, even smaller ones like unit Cp$_9$ and CP$_{17}$, or CP$_{12}$–CP$_{14}$. With the assumption that the reflectors are present due to an interbedded thin manteling/sediment layer (Morgan et al., 2015), the finding suggests that there was enough time in between the eruptions to deposit material and thus, the units are likely not associated with the same eruption, such as late stage flow breakout.

The architecture, thicknesses, and volumes in Elysium Planitia are similar to terrestrial flood basalts on Earth. For example, the youngest and best-preserved continental flood basalt on Earth, the Columbia River Basalt Group (CRBG), is divided into five formations (e.g., Reidel, 2015; Self et al., 1998; Thordarson & Self, 1998). Similarly, Elysium Planitia can be divided into five major flow units with volumes ranging from 4,000 $\pm$ 1,600 to 16,000 $\pm$ 4,000 km^3, comparable to the CRBG Wanapum formation (12,175 km^3; Self et al., 1998) or the smallest Saddle Mountains Basalts formation (2,424 km^3; Self et al., 1998). Volumes of the Cerberus Plains lava units, for examples the CP$_9$ unit with 1,100 $\pm$ 500 km^3 and CP$_{17}$ unit with 1,700 $\pm$ 240 km^3, are also comparable in volume to members and units of the CRBG, such as the Roza member (1,300 km^3; Self et al., 1998) of the Wanapum Formation, or Sentinel Gap unit (1,190 km^3; Self et al., 1998) within the Frenchman Spring member. Additionally, Cerberus Plains in Elysium Planitia is composed of at least 19 lava flows in addition to lava shields implying multiple eruption sequences over tens of millions of years. This is similar to the CRBG, where members are commonly containing 1 to 20 lava flows each emplaced over millions of years (Reidel, 2015). The total erupted volume of Elysium Planitia; however, is with 95,000 $\pm$ 9,000 km^3 smaller than the erupted volume of ~210,000 km^3 for the CRBG (Reidel, 2015).

7. Conclusions

This study discusses the volcanological and aqueous evolution of Elysium Planitia on Mars. By combining detailed geomorphological mapping and the analysis of SHARAD reflectors we determined individual lava flow areas, thicknesses, and volumes. In the area of 9,126,790 km^2 we found a total of 1,777 SHARAD reflectors. The lava flow-fields within Elysium Planitia have been challenging to reconstruct due to the complex surface morphology and the dynamic flow history of typically shallow, overlapping lava flows, ranging from only 5 m up to 104 m in thickness and average thicknesses of 11 $\pm$ 5–28 $\pm$ 4 m. Multiple locations, including the Cerberus Plains, Marte Vallis, and Rahway Valles contain several stacked reflectors, which indicates episodic volcanic activity resulting in the emplacement of several lava flow-fields, like seen in large flood basalts on Earth, such as the Columbia River Basalt Group (Thordarson & Self, 1998). Evaluating the subsurface reflectors in the context of the detailed geomorphological mapping, we show that Marte Vallis is much larger but also much shallower than previously suggested with a likely paleo-flow direction of the water from northwest to southeast. This paleo-flow direction is the same flow direction of younger infilling lava flows, based on textural kinematic indicators exposed on the surface, which imply a complex history alternating water and lava emplacement. We inferred a lava volume of 12,200 $\pm$ 2,500 km^3 for the youngest Marte Vallis lavas and 4,000 $\pm$ 1,600 km^3 for Athabasca Valles, the latter is consistent with previous estimates. Our results show that the latest materials forming Elysium Planitia are dominated by lava flow-fields formed by effusive eruptions and do not support the interpretation that the large valleys are filled by ice-rice sediment or pure ice. Geomorphologic mapping reveals that all surfaces exhibit features consistent with lava flow emplacement. The real part of the permittivity constrained for the area from dipping reflectors is 7.8 $\pm$ 1 indicating that the valleys carved by fluvial activity have been filled with basalt, with porosity values of 9.5% $\pm$ 5%. However, as evidence for lava–water interactions exists, local ice deposits were almost certainly present in the past and might still persist today. The young volcanic surfaces and the recent detection of seismic activity in Elysium Planitia (e.g., Banerdt et al., 2020; Jacob et al., 2022; Stähler et al., 2022)

could imply that Mars is still volcanically active. With its very recent geologic activity, Elysium Planitia is an exceptionally important region that is vital for understanding the past and current volcanological and magmatic state of Mars in addition to its recent aqueous history.

Data Availability Statement

Data used in this study, including SHARAD (Campbell & Phillips, 2006), CTX (Malin et al., 2007), HiRISE (McEwen et al., 2007), and MOLA (Smith, 1998) are publicly available at Planetary Data System (PDS). Data sets including shapefiles for the ArcGIS-based geomorphological maps and source data for the depth maps for Elysium Planitia on Mars derived in this study are published on the University of Arizona Research Data Repository (Voigt et al., 2023).

References

Arun, P. (2013). A comparative analysis of different DEM interpolation methods. *The Egyptian Journal of Remote Sensing and Space Science*, *16*(2), 133–139. https://doi.org/10.1016/j.ejrs.2013.09.001

Baker, D. M., & Head, J. W. (2015). Extensive Middle Amazonian mantling of debris aprons and plains in Deuteronilus Mensae, Mars: Implications for the record of mid-latitude glaciation. *Icarus*, *260*, 269–288. https://doi.org/10.1016/j.icarus.2015.06.036

Balme, M. R., & Gallagher, C. (2009). An equatorial periglacial landscape on Mars. *Earth and Planetary Science Letters*, *285*(1–2), 1–15. https://doi.org/10.1016/j.epsl.2009.05.031

Banerdt, W. B., Smrekar, S. E., Banfield, D., Giardini, D., Golombek, M., Johnson, C. L., et al. (2020). Initial results from the insight mission on Mars. *Nature Geoscience*, *13*(3), 183–189. https://doi.org/10.1038/s41561-020-0544-y

Barataux, D., Samuel, H., Michaut, C., Toplis, M. J., Monnereau, M., Wieczorek, M., et al. (2014). Petrological constraints on the density of the Martian crust. *Journal of Geophysical Research: Planets*, *119*(7), 1707–1727. https://doi.org/10.1002/2014JE004642

Berman, D. C., & Hartmann, W. K. (2002). Recent fluvial, volcanic, and tectonic activity on the Cerberus Plains of Mars. *Icarus*, *159*(1), 1–17. https://doi.org/10.1006/icar.2002.6920

Berman, D. C., Hartmann, W. K., & Burr, D. M. (2001). Marte Vallis and the Cerberus Plains: Evidence of young water flow on Mars. In *Lunar and planetary science conference* (Conference Paper No. 1732).

Boivin, A. L., Tsai, C.-A., Hickson, D. C., Ghent, R. R., & Daly, M. G. (2022). Determination of broadband complex EM parameters of powdered materials: 2. Ilmenite-bearing lunar analogue materials. *Journal of Geophysical Research: Planets*, *127*(10), e2022JE007200. https://doi.org/10.1029/2022JE007200

Broquet, A., & Andrews-Hanna, J. C. (2023). Geophysical evidence for an active mantle plume underneath Elysium Planitia on Mars. *Nature Astronomy*, *7*, 160–169. https://doi.org/10.1038/s41550-022-01836-3

Brown, J. R., & Roberts, G. P. (2023). Repeated, cross-cutting, and spatially migrating outflow channel formation, Grjótá Valles, Mars. *Journal of Geophysical Research: Planets*, *128*(2), e2022JE007247. https://doi.org/10.1029/2022JE007247

Burr, D. M., Enga, M.-T., Williams, R. M. E., Zimbelman, J. R., Howard, A. D., & Brennand, T. A. (2009). Pervasive aqueous paleoflow features in the Aeolis/Zephyria Plana region, Mars. *Icarus*, *200*(1), 52–76. https://doi.org/10.1016/j.icarus.2008.10.014

Burr, D. M., Grier, J. A., McEwen, A. S., & Keszthelyi, L. P. (2002). Repeated aqueous flooding from the Cerberus Fossae: Evidence for very recently extant, deep groundwater on Mars. *Icarus*, *159*(1), 53–73. https://doi.org/10.1006/icar.2002.6921

Burr, D. M., & McEwen, A. S. (2000). Improved discharge calculations for the Cerberus region, Mars. *Eos*, *81*, 19.

Burr, D. M., Soare, R. J., Wan Bun Tseung, J.-M., & Emery, J. P. (2005). Young (late Amazonian), near-surface, ground ice features near the equator, Athabasca Valles, Mars. *Icarus*, *178*(1), 56–73. https://doi.org/10.1016/j.icarus.2005.04.012

Campbell, B. A., Carter, L., Phillips, R., Plaut, J., Putzig, N., Safaeinili, A., et al. (2008). SHARAD radar sounding of the Vastitas Borealis formation in Amazonis Planitia. *Journal of Geophysical Research*, *113*(E12), E12010. https://doi.org/10.1029/2008JE003177

Campbell, B. A., & Phillips, R. (2006). Mars reconnaissance orbiter shallow radar radargram data, MRO-M-SHARAD-5-RADARGRAM-V2.0. *NASA Planetary Data System*. https://doi.org/10.17189/YB1W-F075

Campbell, B. A., Watters, T. R., & Morgan, G. A. (2021). Dielectric properties of the Medusae Fossae formation and implications for ice content. *Journal of Geophysical Research: Planets*, *126*(3), e2020JE006601. https://doi.org/10.1029/2020JE006601

Carr, M. H. (2007). *The surface of Mars*. Cambridge University Press.

Carter, L. M., Campbell, B. A., Watters, T. R., Phillips, R. J., Putzig, N. E., Safaeinili, A., et al. (2009). Shallow radar (SHARAD) sounding observations of the Medusae Fossae formation, Mars. *Icarus*, *199*(2), 295–302. https://doi.org/10.1016/j.icarus.2008.10.007

Choudhary, P., Holt, J. W., & Kempf, S. D. (2016). Surface clutter and echo location analysis for the interpretation of SHARAD data from Mars. *IEEE Geoscience and Remote Sensing Letters*, *13*(9), 1285–1289. https://doi.org/10.1109/LGRS.2016.2581799

Clifford, S., Crisp, D., Fisher, D., Herkenhoff, K., Smrekar, S., Thomas, P., & Zwally, H. J. (2000). The state and future of Mars polar science and exploration. *Icarus*, *144*(2), 210–242. https://doi.org/10.1006/icar.1999.6290

Dickson, J. L., Ehlmann, B. L., Kerber, L. H., & Fassett, C. I. (2023). Release of the global CTX mosaic of Mars: An experiment in information-preserving image data processing. In *LPI contributions*. Retrieved from https://www.hou.usra.edu/meetings/lpsc2023/pdf/2353.pdf

Dickson, J. L., Kerber, L. A., Fassett, C. I., & Ehlmann, B. L. (2018). A global, blended CTX mosaic of Mars with vectorized seam mapping: A new mosaicking pipeline using principles of non-destructive image editing. In *Lunar and Planetary Institute*. Retrieved from https://ui.adsabs.harvard.edu/\#abs/2018LPI…49.2480D

Fagents, S. A., Lanagan, P., & Greeley, R. (2002). Rootless cones on Mars: A consequence of lava-ground ice interaction. *Geological Society, London, Special Publications*, *202*(1), 295–317. https://doi.org/10.1144/GSL.SP.2002.202.01.15

Fagents, S. A., & Thordarson, T. (2007). Rootless volcanic cones in Iceland and on Mars. In M. Chapman (Ed.), *The geology of Mars: Evidence from Earth-based analogs* (pp. 151–177). Cambridge University Press. https://doi.org/10.1017/CBO9780511536014.007

Fastook, J. L., Head, J. W., Forget, F., Madeleine, J.-B., & Marchant, D. R. (2011). Evidence for Amazonian northern mid-latitude regional glacial landsystems on Mars: Glacial flow models using GCM-driven climate results and comparisons to geological observations. *Icarus*, *216*(1), 23–39. https://doi.org/10.1016/j.icarus.2011.07.018

Feldman, W. C., Prettyman, T. H., Maurice, S., Plaut, J. J., Bish, D. L., Vaniman, D. T., et al. (2004). Global distribution of near-surface hydrogen on Mars. *Journal of Geophysical Research*, *109*(E9), E09006. https://doi.org/10.1029/2003JE002160

Filiberto, J., Baratoux, D., Beaty, D., Breuer, D., Farcy, B. J., Grott, M., et al. (2016). A review of volatiles in the Martian interior. *Meteoritics & Planetary Sciences*, *51*(11), 1935–1958. https://doi.org/10.1111/maps.12680

Fischer, T. P. (2008). Fluxes of volatiles (H_2O, CO_2, N_2, Cl, F) from arc volcanoes. *Geochemical Journal*, *42*(1), 21–38. https://doi.org/10.2343/geochemj.42.21

Forget, F., Haberle, R. M., Montmessin, F., Levrard, B., & Head, J. W. (2006). Formation of glaciers on Mars by atmospheric precipitation at high obliquity. *Science*, *311*(5759), 368–371. https://doi.org/10.1126/science.1120335

Frey, H. (1987). *Pseudocraters as indicators of ground ice on Mars*. Reports of Planetary Geology and Geophysics Program, 1986. NASA.

Fuller, E. R., & Head, J. W. (2002). Amazonis Planitia: The role of geologically recent volcanism and sedimentation in the formation of the smoothest plains on Mars. *Journal of Geophysical Research*, *107*(E10), 11-1–11-25. https://doi.org/10.1029/2002je001842

Gleick, P. (1996). Water resources. Encyclopedia of climate. *Weather*, 817–823. Retrieved from https://cir.nii.ac.jp/crid/1574231875534157696

Golder, K. B., Burr, D. M., & Kattenhorn, S. A. (2020). Investigation of target property effects on crater populations in long lava flows: A study in the Cerberus region, Mars, with implications for magma source identification. *Icarus*, *335*, 113388. https://doi.org/10.1016/j.icarus.2019.113388

Hamid, S., Kerber, L., & Clarke, A. B. (2023). Volcanic degassing a potential source of surface water ice near Martian volcanoes. In *LPI contributions*. Retrieved from https://www.hou.usra.edu/meetings/lpsc2023/pdf/2890.pdf

Hamilton, C. W., Fagents, S. A., & Thordarson, T. (2011). Lava–ground ice interactions in Elysium Planitia, Mars: Geomorphological and geospatial analysis of the Tartarus Colles cone groups. *Journal of Geophysical Research*, *116*(E3), E03004. https://doi.org/10.1029/2010JE003657

Hamilton, C. W., Fagents, S. A., & Wilson, L. (2010). Explosive lava-water interactions in Elysium Planitia, Mars: Geologic and thermodynamic constraints on the formation of the Tartarus Colles cone groups. *Journal of Geophysical Research*, *115*(E9), E09006. https://doi.org/10.1029/2009je003546

Hamilton, C. W., Fitch, E. P., Fagents, S. A., & Thordarson, T. (2017). Rootless tephra stratigraphy and emplacement processes. *Bulletin of Volcanology*, *79*(1), 11. https://doi.org/10.1007/s00445-016-1086-4

Hamilton, C. W., Glaze, L. S., James, M. R., & Baloga, S. M. (2013). Topographic and stochastic influences on pāhoehoe lava lobe emplacement. *Bulletin of Volcanology*, *75*(11), 756. https://doi.org/10.1007/s00445-013-0756-8

Harish, Kimi, K., Tuhi, S., Baliyan, S., Mangold, N., Vijayan, S., & El-Maarry, M. (2023). Shallow subsurface basalt layer along Cerberus Fossae, Mars: Insights from SHARAD, HiRISE, and CRISM analysis. *Icarus*, *391*, 115343. https://doi.org/10.1016/j.icarus.2022.115343

Hauber, E., van Gasselt, S., Chapman, M. G., & Neukum, G. (2008). Geomorphic evidence for former lobate debris aprons at low latitudes on Mars: Indicators of the Martian paleoclimate. *Journal of Geophysical Research*, *113*(E2), E02007. https://doi.org/10.1029/2007je002897

Head, J. W., & Marchant, D. R. (2003). Cold-based mountain glaciers on Mars: Western Arsia Mons. *Geology*, *31*(7), 641–644. https://doi.org/10.1130/0091-7613(2003)031⟨0641:cmgomw⟩2.0.co;2

Holt, J. W., Safaeinili, A., Plaut, J. J., Head, J. W., Phillips, R. J., Seu, R., et al. (2008). Radar sounding evidence for buried glaciers in the southern mid-latitudes of Mars. *Science*, *322*(5905), 1235–1238. https://doi.org/10.1126/science.1164246

Jacob, A., Plasman, M., Perrin, C., Fuji, N., Lognonné, P., Xu, Z., et al. (2022). Seismic sources of insight marsquakes and seismotectonic context of Elysium Planitia, Mars. *Tectonophysics*, *837*, 229434. https://doi.org/10.1016/j.tecto.2022.229434

Jaeger, W. L., Keszthelyi, L. P., McEwen, A. S., Dundas, C. M., & Russell, P. S. (2007). Athabasca Valles, Mars: A lava-draped channel system. *Science*, *317*(5845), 1709–1711. https://doi.org/10.1126/science.1143315

Jaeger, W. L., Keszthelyi, L. P., Skinner, J. A., Jr., Milazzo, M. P., McEwen, A. S., Titus, T. N., et al. (2010). Emplacement of the youngest flood lava on Mars: A short, turbulent story. *Icarus*, *205*(1), 230–243. https://doi.org/10.1016/j.icarus.2009.09.011

Jaumann, R., Neukum, G., Behnke, T., Duxbury, T. C., Eichentopf, K., Flohrer, J., et al. (2007). The high-resolution stereo camera (HRSC) experiment on Mars Express: Instrument aspects and experiment conduct from interplanetary cruise through the nominal mission. *Planetary and Space Science*, *55*(7–8), 928–952. https://doi.org/10.1016/j.pss.2006.12.003

Karlsson, H. R., Clayton, R. N., Gibson, E. K., & Mayeda, T. K. (1992). Water in SNC meteorites: Evidence for a Martian hydrosphere. *Science*, *255*(5050), 1409–1411. https://doi.org/10.1126/science.11537889

Kerber, L., & Head, J. W. (2010). The age of the Medusae Fossae formation: Evidence of Hesperian emplacement from crater morphology, stratigraphy, and ancient lava contacts. *Icarus*, *206*(2), 669–684. https://doi.org/10.1016/j.icarus.2009.10.001

Kerber, L., Head, J. W., Madeleine, J.-B., Forget, F., Wilson, L., & Levine, J. (2011). Explosive volcanic eruptions into the Martian atmosphere: Tracking ash and water ice. In *42nd annual lunar and planetary science conference*. Retrieved from https://www.lpi.usra.edu/meetings/lpsc2011/pdf/2015.pdf

Keszthelyi, L., Huff, A., & Jaeger, W. (2021). Geologic map of the Athabasca Valles region, Mars: U.S. Geological Survey scientific investigations map 3477. https://doi.org/10.3133/sim3477

Keszthelyi, L., McEwen, A. S., & Thordarson, T. (2000). Terrestrial analogs and thermal models for Martian flood lavas. *Journal of Geophysical Research*, *105*(E6), 15027–15049. https://doi.org/10.1029/1999je001191

Keszthelyi, L., Thordarson, T., McEwen, A., Haack, H., Guilbaud, M.-N., Self, S., & Rossi, M. J. (2004). Icelandic analogs to Martian flood lavas. *Geochemistry, Geophysics, Geosystems*, *5*(11), Q11014. https://doi.org/10.1029/2004GC000758

Kiefer, W. S. (2003). Melting in the Martian mantle: Shergottite formation and implications for present-day mantle convection on Mars. *Meteoritics & Planetary Sciences*, *38*(12), 1815–1832. https://doi.org/10.1111/j.1945-5100.2003.tb00017.x

Kiefer, W. S., Macke, R. J., Britt, D. T., Irving, A. J., & Consolmagno, G. J. (2014). The density, porosity, and magnetic susceptibility of Martian meteorites as constraints on gravity models. Retrieved from https://www.hou.usra.edu/meetings/lpsc2014/pdf/2028.pdf

Kneissl, T., van Gasselt, S., & Neukum, G. (2011). Map-projection-independent crater size-frequency determination in GIS environments–new software tool for ArcGIS. *Planetary and Space Science*, *59*(11–12), 1243–1254. https://doi.org/10.1016/j.pss.2010.03.015

Lanagan, P. D., McEwen, A. S., Keszthelyi, L. P., & Thordarson, T. (2001). Rootless cones on Mars indicating the presence of shallow equatorial ground ice in recent times. *Geophysical Research Letters*, *28*(12), 2365–2367. https://doi.org/10.1029/2001gl012932

Laskar, J., Correia, A. C. M., Gastineau, M., Joutel, F., Levrard, B., & Robutel, P. (2004). Long term evolution and chaotic diffusion of the insolation quantities of Mars. *Icarus*, *170*(2), 343–364. https://doi.org/10.1016/j.icarus.2004.04.005

Madeleine, J. B., Forget, F., Head, J. W., Levrard, B., Montmessin, F., & Millour, E. (2009). Amazonian northern mid-latitude glaciation on Mars: A proposed climate scenario. *Icarus*, *203*(2), 390–405. https://doi.org/10.1016/j.icarus.2009.04.037

Malin, M. C., Bell, J. F., Cantor, B. A., Caplinger, M. A., Calvin, W. M., Clancy, R. T., et al. (2007). Context camera investigation on board the Mars Reconnaissance Orbiter. *Journal of Geophysical Research*, *112*(E5), E05S04. https://doi.org/10.1029/2006je002808

Manga, M., & Wright, V. (2021). No cryosphere-confined aquifer below insight on Mars. *Geophysical Research Letters*, *48*(8), e2021GL093127. https://doi.org/10.1029/2021GL093127

McCoy, T. J., Corrigan, C. M., & Herd, C. D. K. (2011). Combining meteorites and missions to explore Mars. *Proceedings of the National Academy of Sciences of the United States of America*, *108*(48), 19159–19164. https://doi.org/10.1073/pnas.1013478108

McEwen, A. S., Eliason, E. M., Bergstrom, J. W., Bridges, N. T., Hansen, C. J., Delamere, W. A., et al. (2007). Mars reconnaissance orbiter's high resolution imaging science experiment (HIRISE). *Journal of Geophysical Research*, *112*(E5), E05S02. https://doi.org/10.1029/2005je002605

McEwen, A. S., Preblich, B. S., Turtle, E. P., Artemieva, N. A., Golombek, M. P., Hurst, M., et al. (2005). The rayed crater Zunil and interpretations of small impact craters on Mars. *Icarus*, *176*(2), 351–381. https://doi.org/10.1016/j.icarus.2005.02.009

McSween, H. Y., Grove, T. L., Lentz, R. C., Dann, J. C., Holzheid, A. H., Riciputi, L. R., & Ryan, J. G. (2001). Geochemical evidence for magmatic water within Mars from pyroxenes in the Shergotty meteorite. *Nature*, *409*(6819), 487–490. https://doi.org/10.1038/35054011

Michael, G. G. (2013). Planetary surface dating from crater size–frequency distribution measurements: Multiple resurfacing episodes and differential isochron fitting. *Icarus*, *226*(1), 885–890. https://doi.org/10.1016/j.icarus.2013.07.004

Michael, G. G., & Neukum, G. (2010). Planetary surface dating from crater size-frequency distribution measurements: Partial resurfacing events and statistical age uncertainty. *Earth and Planetary Science Letters*, *294*(3–4), 223–229. https://doi.org/10.1016/j.epsl.2009.12.041

Morgan, G. A., Campbell, B. A., Carter, L. M., & Plaut, J. J. (2015). Evidence for the episodic erosion of the Medusae Fossae formation preserved within the youngest volcanic province on Mars. *Geophysical Research Letters*, *42*(18), 7336–7342. https://doi.org/10.1002/2015gl065017

Morgan, G. A., Campbell, B. A., Carter, L. M., Plaut, J. J., & Phillips, R. J. (2013). 3D reconstruction of the source and scale of buried young flood channels on Mars. *Science*, *340*(6132), 607–610. https://doi.org/10.1126/science.1234787

Murray, J. B., Muller, J.-P., Neukum, G., Werner, S. C., Hauber, E., Markiewicz, W. J., et al. (2005). Evidence from HRSC Mars Express for a frozen sea close to Mars' equator. In *Lunar and planetary science XXXVI*. Retrieved from http://adsabs.harvard.edu/abs/2005LPI…36.1741M

Mustard, J., Murchie, S. L., Pelkey, S. M., Ehlmann, B. L., Milliken, R. E., Grant, J. A., et al. (2008). Hydrated silicate minerals on Mars observed by the Mars reconnaissance orbiter CRISM instrument. *Nature*, *454*(7202), 305–309. https://doi.org/10.1038/nature07097

Noguchi, R., & Kurita, K. (2015). Unique characteristics of cones in central Elysium Planitia, Mars. *Planetary and Space Science*, *111*, 44–54. https://doi.org/10.1016/j.pss.2015.03.007

Ojha, L., Lewis, K., Karunatillake, S., & Schmidt, M. (2018). The Medusae Fossae formation as the single largest source of dust on Mars. *Nature Communications*, *9*(1), 1–7. https://doi.org/10.1038/s41467-018-05291-5

Paladino, T., Nawotniak, S., Kerber, L., Millour, E., & Karunatillake, S. (2023). Ancient volcanism may have influenced patterns of hydrated regolith on Mars. In *LPI contributions*. Retrieved from https://www.hou.usra.edu/meetings/lpsc2023/pdf/2431.pdf

Palumbo, A. M., & Head, J. W. (2020). Groundwater release on early Mars: Utilizing models and proposed evidence for groundwater release to estimate the required climate and subsurface water budget. *Geophysical Research Letters*, *47*(8), e2020GL087230. https://doi.org/10.1029/2020GL087230

Petersen, E. I., Holt, J. W., & Levy, J. S. (2018). High ice purity of Martian lobate debris aprons at the regional scale: Evidence from an orbital radar sounding survey in Deuteronilus and Protonilus Mensae. *Geophysical Research Letters*, *45*(21), 11595–11604. https://doi.org/10.1029/2018GL079759

Platz, T., & Michael, G. (2011). Eruption history of the Elysium volcanic province, Mars. *Earth and Planetary Science Letters*, *312*(1–2), 140–151. https://doi.org/10.1016/j.epsl.2011.10.001

Plescia, J. B. (2003). Cerberus Fossae, Elysium, Mars: A source for lava and water. *Icarus*, *164*(1), 79–95. https://doi.org/10.1016/s0019-1035(03)00139-8

Posiolova, L. V., Lognonné, P., Banerdt, W. B., Clinton, J., Collins, G. S., Kawamura, T., et al. (2022). Largest recent impact craters on Mars: Orbital imaging and surface seismic co-investigation. *Science*, *378*(6618), 412–417. https://doi.org/10.1126/science.abq7704

Poulet, F., Bibring, J.-P., Langevin, Y., Gondet, B., Mustard, J., Gendrin, A., et al. (2006). The distribution of phyllosilicates on Mars from the omega-mex imaging spectrometer. In *37th annual lunar and planetary science conference*. Retrieved from http://adsabs.harvard.edu/abs/2006LPI…37.1698P

Ramsdale, J. D., Balme, M. R., Conway, S. J., & Gallagher, C. (2015). Ponding, draining and tilting of the Cerberus Plains; a cryolacustrine origin for the sinuous ridge and channel networks in Rahway Vallis, Mars. *Icarus*, *253*, 256–270. https://doi.org/10.1016/j.icarus.2015.03.005

Reidel, S. P. (2015). Igneous rock associations 15. The Columbia River Basalt group: A flood basalt province in the Pacific northwest, USA. *Geoscience Canada*, *42*(1), 151–168. https://doi.org/10.12789/geocanj.2014.41.061

Richardson, J. A., Bleacher, J. E., Connor, C. B., & Glaze, L. S. (2021). Small volcanic vents of the Tharsis volcanic province, Mars. *Journal of Geophysical Research: Planets*, *126*(2), e2020JE006620. https://doi.org/10.1029/2020JE006620

Schumacher, S., & Breuer, D. (2007). An alternative mechanism for recent volcanism on Mars. *Geophysical Research Letters*, *34*(14), L14202. https://doi.org/10.1029/2007GL030083

Self, S., Keszthelyi, L., & Thordarson, T. (1998). The importance of pāhoehoe. *Annual Review of Earth and Planetary Sciences*, *26*(1), 81–110. https://doi.org/10.1146/annurev.earth.26.1.81

Seu, R., Biccari, D., Cartacci, M., Cicchetti, A., Fuga, O., Giuppi, S., et al. (2007). The shallow radar (SHARAD) experiment, a subsurface sounding radar for MRO. *Memorie della Societa Astronomica Italiana Supplement*, *11*, 26. Retrieved from http://adsabs.harvard.edu/abs/2007MSAIS..11…26S

Shoemaker, E. S., Carter, L. M., Garry, W. B., Morgan, G. A., & Plaut, J. J. (2022). New insights into subsurface stratigraphy Northwest of Ascraeus Mons, Mars, using the SHARAD and MARSIS radar sounders. *Journal of Geophysical Research: Planets*, *127*(6), e2022JE007210. https://doi.org/10.1029/2022JE007210

Simon, M. N., Carter, L. M., Campbell, B. A., Phillips, R. J., & Mattei, S. (2014). Studies of lava flows in the Tharsis region of Mars using SHARAD. *Journal of Geophysical Research: Planets*, *119*(11), 2291–2299. https://doi.org/10.1002/2014JE004666

Sivia, D., & Skilling, J. (2006). *Data analysis: A Bayesian tutorial* (2nd ed.). Oxford University Press.

Smith, D. E. (1998). Mgs sampler Mars orbiter laser altimeter PEDR ASCII tables. *NASA Planetary Data System*. https://doi.org/10.17189/1519449

Smith, D. E., Zuber, M. T., Frey, H. V., Garvin, J. B., Head, J. W., Muhleman, D. O., et al. (2001). Mars orbiter laser altimeter: Experiment summary after the first year of global mapping of Mars. *Journal of Geophysical Research*, *106*(E10), 23689–23722. https://doi.org/10.1029/2000je001364

Stähler, S. C., Mittelholz, A., Perrin, C., Kawamura, T., Kim, D., Knapmeyer, M., et al. (2022). Tectonics of Cerberus Fossae unveiled by marsquakes. *Nature Astronomy*, *6*(12), 1376–1386. https://doi.org/10.1038/s41550-022-01803-y

Stillman, D. E., & Grimm, R. E. (2011). Radar penetrates only the youngest geological units on Mars. *Journal of Geophysical Research*, *116*(E3), E03001. https://doi.org/10.1029/2010JE003661

Stillman, D. E., & Olhoeft, G. (2008). Frequency and temperature dependence in electromagnetic properties of Martian analog minerals. *Journal of Geophysical Research*, *113*(E9), E09005. https://doi.org/10.1029/2007JE002977

Stockstill-Cahill, K., Anderson, F. S., & Hamilton, V. (2008). A study of low-albedo deposits within amazonis planitia craters: Evidence for locally derived ultramafic to mafic materials. *Journal of Geophysical Research*, *113*(E7), 07008. https://doi.org/10.1029/2007JE003036

Tanaka, K. L. (2014). The new geologic map of Mars: Guiding research and education. *Eos, Transactions American Geophysical Union*, *95*(38), 341–342. https://doi.org/10.1002/2014eo380001

Tanaka, K. L., Skinner, J. A., & Hare, T. M. (2005). Geologic map of the northern plains of Mars.

Thordarson, T., & Self, S. (1998). The Roza Member, Columbia River Basalt group: A gigantic pahoehoe lava flow field formed by endogenous processes? *Journal of Geophysical Research*, *103*(B11), 27411–27445. https://doi.org/10.1029/98JB01355

Ulaby, F., Bengal, T., East, J., Dobson, M., Garvin, J., & Evans, D. (1988). Microwave dielectric spectrum of rocks. In *Technical memorandum*.

Vaucher, J., Baratoux, D., Mangold, N., Pinet, P., Kurita, K., & Gregoire, M. (2009). The volcanic history of central Elysium Planitia: Implications for Martian magmatism. *Icarus*, *204*(2), 418–442. https://doi.org/10.1016/j.icarus.2009.06.032

Vaucher, J., Baratoux, D., Toplis, M. J., Pinet, P., Mangold, N., & Kurita, K. (2009). The morphologies of volcanic landforms at central Elysium Planitia: Evidence for recent and fluid lavas on Mars. *Icarus*, *200*(1), 39–51. https://doi.org/10.1016/j.icarus.2008.11.005

Voigt, J. R. C., & Hamilton, C. W. (2018). Investigating the volcanic versus aqueous origin of the surficial deposits in eastern Elysium Planitia, Mars. *Icarus*, *309*, 389–410. https://doi.org/10.1016/j.icarus.2018.03.009

Voigt, J. R. C., Hamilton, C. W., Scheidt, S. P., Munzer, U., Hoskuldsson, A., Jonsdottir, I., & Thordarson, T. (2021). Geomorphological characterization of the 2014–2015 Holuhraun lava flow-field in Iceland. *Journal of Volcanology and Geothermal Research*, *419*, 107278. https://doi.org/10.1016/j.jvolgeores.2021.107278

Voigt, J. R. C., Hamilton, C. W., & Steinbrügge, G. (2023). Geomorphological maps and depth maps for Elysium Planitia, Mars [Dataset]. University of Arizona Research Data Repository. https://doi.org/10.25422/azu.data.23278289

Voigt, J. R. C., Hamilton, C. W., Steinbrügge, G., Hoskuldsson, A., Jonsdottir, I., & Thordarson, T. (2022). Linking effusion rates and lava morphologies for the 2014–2015 Holuhraun lava flow-field in Iceland. *Geology*, *50*(1), 71–75. https://doi.org/10.1130/G49251.1

Voigt, J. R. C., Hamilton, C. W., Steinbrügge, G., & Scheidt, S. P. (2021). Surface roughness characterization of the 2014–2015 Holuhraun lava flow-field in Iceland: Implications for facies mapping and remote sensing. *Bulletin of Volcanology*, *82*. https://doi.org/10.1007/s00445-021-01499-4

Wackernagel, H. (1995). Ordinary kriging. In *Multivariate geostatistics: An introduction with applications* (pp. 74–81). Springer Berlin Heidelberg. https://doi.org/10.1007/978-3-662-03098-1_11

Watters, T. R., Campbell, B., Carter, L., Leuschen, C. J., Plaut, J. J., Picardi, G., et al. (2007). Radar sounding of the Medusae Fossae formation Mars: Equatorial ice or dry, low-density deposits? *Science*, *318*(5853), 1125–1128. https://doi.org/10.1126/science.1148112

Wilson, L., & Head, J. (2009). Tephra deposition on glaciers and ice sheets on Mars: Influence on ice survival, debris content and flow behavior. *Journal of Volcanology and Geothermal Research*, *185*(4), 290–297. https://doi.org/10.1016/j.jvolgeores.2008.10.003

Wright, V., Dasent, J., Kilburn, R., & Manga, M. (2022). A minimally cemented shallow crust beneath insight. *Geophysical Research Letters*, *49*(15), e2022GL099250. https://doi.org/10.1029/2022GL099250

Xiong, S., Tao, Y., Persaud, D. M., Campbell, J. D., Putri, A. R. D., & Muller, J.-P. (2021). Subsurface reflectors detected by SHARAD reveal stratigraphy and buried channels over central Elysium Planitia, Mars. *Earth and Space Science*, *8*(1), e2019EA000968. https://doi.org/10.1029/2019EA000968